CHARACTERIZATION OF ATMOSPHERIC NOISE AND PRECIPITATION STATIC IN THE LONG RANGE NAVIGATION (LORAN-C) BAND FOR AIRCRAFT

A thesis presented to
the faculty of the College of Engineering and Technology of
Ohio University

In partial fulfillment
of the requirements for the degree
Master of Science

Manish Lad

August 2004

This thesis entitled

CHARACTERIZATION OF ATMOSPHERIC NOISE AND PRECIPITATION STATIC IN THE LONG RANGE NAVIGATION (LORAN-C) BAND FOR AIRCRAFT

By

Manish Lad

has been approved for

The School of Electrical Engineering and Computer Science

and the Russ College of Engineering and Technology by

Frank van Graas

Fritz J. and Dolores H. Russ Professor of Electrical Engineering

R. Dennis Irwin

Dean, Russ College of Engineering and Technology

# ABSTRACT

Lad, Manish. M.S. August 2004. Electrical Engineering

Characterization of Atmospheric Noise and Precipitation Static in the Long Range Navigation (Loran-C) Band for Aircraft (98 pp.)

Director of Thesis: Frank van Graas

This Thesis investigates the effects of noise caused by lightning discharges and Precipitation Static (P-Static) in the Loran-C band, as observed by an airborne receiver.

To characterize the noise, an airborne data collection system was used to store the radio frequency samples from both a loop (H-field) antenna and a wire (E-field) antenna. Flight test data were collected and analyzed under nominal, P-Static, and nearby thunderstorm conditions.

Based on the research described in this thesis it was found that: 1) E-field and H-field antennas are affected similarly by lightning-induced noise; 2) In the presence of thunderstorms, the noise increase for both antennas was less than 2.3 dB; and 3) An H-field antenna effectively mitigates aircraft P-Static noise in the Loran-C band.

Approved:

Frank van Graas

Fritz J. and Dolores H. Russ Professor of Electrical Engineering

ACKNOWLEDGEMENTS

The work presented in this thesis was funded by the Federal Aviation Administration (FAA), under contract DTFA01-01-C-00071, Technical Task Directive 2.1 – Loran-C Analysis and Support. I would like to thank the Program Office Manager, Mr. Mitchell Narins, for his assistance in making this research possible.

I would like to express my utmost gratitude to Dr. Frank van Graas for his unending support, guidance and encouragement throughout this work. His insight and expertise in different navigation systems was invaluable. I have learned much under his guidance and he has given me many opportunities to expand my knowledge base. I am truly fortunate to have worked with him.

I would also like to thank Dr. Chris Bartone, Dr. David Diggle, and Dr. Gene Kaufman for reviewing this document and serving as members of the Thesis committee. The help and assistance provided by the staff and students of the Avionics Engineering Center in flight-testing and other areas will also not be forgotten. In particular, Curtis Cutright and Dr. David Diggle are thanked for their technical help and guidance.

Finally, words alone cannot express the thanks I owe to my family for their encouragement and support. Without them and a blessing from the one above, it would not have been possible.

TABLE OF CONTENTS

LIST OF FIGURES

LIST OF TABLES

LIST OF ACRONYMS

LORAN	LOng RAnge Navigation
LORIPP	Loran Integrity Performance Panel
GRI	Group Repetition Interval
PCI	Phase Code Interval
P-Static	Precipitation Static
NB	Narrow Band
CW	Continuous Wave
NEUS	North East U.S. Loran Chain
GL	Great Lakes Loran Chain
SEUS	South East U.S. Loran Chain
RMS	Root Mean Square
SNR	Signal-to-Noise Ratio
M	Master
V	Victor (Secondary Station)
W	Whiskey (Secondary Station)
X	X-ray (Secondary Station)
Y	Yankee (Secondary Station)
Z	Zulu (Secondary Station)
RF	Radio Frequency
Hz	Hertz
kHz	Kilohertz
MHz	Megahertz
s, ms, µs	Second, millisecond, microsecond
dB	Decibel
CDF	Cumulative distribution function
LPF	Low-pass filter
BPF	Band-pass filter

1 INTRODUCTION

LOng RAnge Navigation (Loran) has been in use since World War II as a positioning, timing, and data broadcast system. Loran-C is the third version of the system since its advent. Loran-C is a ground-based radionavigation system operating in the radio frequency spectrum of 90 to 110 kHz. The system uses groundwave propagation as its primary means of transmission and is therefore not limited to line-of-sight range for its users. Loran-C provides navigation services for both civil and military, air, land and maritime users. It is approved as an en route supplemental air navigation system for both Instrument Flight Rule (IFR) and Visual Flight Rule (VFR) operations [8]. Recent concerns regarding the vulnerability of the satellite-based Global Positioning System (GPS) have led to the evaluation of current and enhanced capabilities of Loran-C to augment GPS.

Use of Loran-C as an airborne radionavigation system has been hampered by concerns in all four key navigation performance parameters: Accuracy, integrity, availability, and continuity. In order to evaluate Loran's potential as a backup system, The Loran Integrity Performance Panel (LORIPP) was formed by the Federal Aviation Administration (FAA) Loran-C Program office. As a member of this panel, the Avionics Engineering Center at Ohio University was tasked to evaluate the effects of atmospheric noise and Precipitation Static (P-Static) on Loran-C performance.

Noise in the Loran-C band consists of atmospheric noise, man-made noise, P-Static noise, and thermal noise. The source of atmospheric noise is lightning discharges produced by thunderstorms occurring worldwide. Atmospheric noise varies with the time of day, the season, geographic location and frequency [19]. Man-made noise includes noise generated by electric motors, power lines, and ignition systems. P-Static is caused by rain, hail, snow, or dust around the reception antenna that gives rise to charge build-ups on the aircraft and associated discharges. For Loran-C, thermal noise, which is caused by thermal agitation of electrons in resistances, is relatively small compared to all other noise sources, but becomes significant for reception antennas with a small effective height, thus requiring a high level of signal amplification.

To characterize atmospheric noise and P-Static noise, flight data were collected using a radio frequency (RF) sampling receiver connected to both wire (E-Field) and loop (H-Field) antennas. This thesis presents the airborne data collection system, data analysis, and results of the data collected under varying flight conditions.

The next chapter provides the Loran-C system overview, which is followed by Chapter 3 on the flight test equipment set up. Signal processing details are contained in Chapter 4. Chapters 5, 6, and 7 present the results obtained from data collected under normal, thunderstorm, and P-Static flight conditions, respectively. Conclusions are drawn in Chapter 8 and recommendations for future work are provided in Chapter 9.

2 LORAN-C SYSTEM OVERVIEW

Loran-C is a low-frequency, land-based radionavigation aid capable of providing two-dimensional (horizontal) positioning, timing, and data broadcast. The basic applications of Loran-C are navigation, communication, precise timing, and frequency reference. In the remainder of this thesis, Loran refers to the current system Loran-C.

2.1 Loran-C Operation and Signal Structure

This section briefly describes the Loran-C operation and signal structure as specified in [1]. For a more detailed description of the signal specification and propagation characteristics, the reader is referred to [1].

The basic Loran-C system consists of a chain of three or more transmitters. Each chain has a designated Master station (M) and two-to-five Secondary stations, designated as Victor (V), Whiskey (W), X-ray (X), Yankee (Y), and Zulu (Z). Each transmitter in the Loran-C chain broadcasts a sequence of pulses within a 20 kHz bandwidth centered around 100 kHz. A pulse is approximately 250 μsec long and the carrier envelope of each pulse rises from zero to maximum amplitude within 65 μsec and then decays for the remainder of the pulse duration. A normal pulse with zero-degree carrier phase is shown in Figure 2.1. The standard Loran pulse waveform can be mathematically described by the following expression [1]:

$$i(t) = 0 \,; \quad \text{for} \quad t < \tau \tag{2.1}$$

$$i(t) = A\left(\frac{t-\tau}{65}\right)^2 \exp\left[\frac{-2(t-\tau)}{65}\right]\sin(\omega t + \varphi); \qquad \text{for } \tau \le t \le 65+\tau \tag{2.2}$$

where:

A: Constant related to peak current (in amperes)

t: Time (μs)

φ: Phase code (radians) which is 0 for positive phase code and π for negative phase code

τ: Envelope-to-cycle difference (μs)

ω: Carrier frequency (0.2π rad/μs)

The accurate time of transmission of a Loran signal is related to the third positive-going zero-crossing (30 μs point) of the pulse. A Loran receiver tracks this zero crossing to determine the time of arrival (TOA) of a pulse. This is illustrated in Figure 2.1. At the 30 μs timing reference point the pulse envelope is at half its peak amplitude and should not experience skywave contamination.

The Master station transmits a series of nine pulses; eight pulses are spaced 1 ms apart while the ninth pulse is 2 ms apart from the eighth pulse. Secondaries transmit a series of eight pulses spaced 1 ms apart. The difference in the number of pulses enables differentiation of master and secondary station signals by a receiver [1]. Figure 2.2 shows the master and the secondary pulse patterns with the timing information. Signal transmission in a chain begins with the pulse group of the Master station. The pulse group of a Master is followed by the pulse groups of Secondary stations. The time interval between successive master station transmissions is termed the Group Repetition Interval (GRI). The GRI is expressed in microseconds and each Loran-C chain has a unique GRI allowing for chain identification. The GRI divided by 10 is used to identify a Loran-C chain.

Within each pulse group, each pulse may be transmitted with a carrier phase of either 0˚ (positive (+) phase code) or 180˚ (negative (-) phase code). Loran signals are transmitted with a fixed phase code sequence which extends over two successive pulse groups and then repeats. This procedure is known as phase coding. Thus, the exact sequence of pulses is matched every two GRIs. This interval is termed the Phase Code Interval (PCI) [1]. The pattern of phase coding is different for master and secondary transmitters.

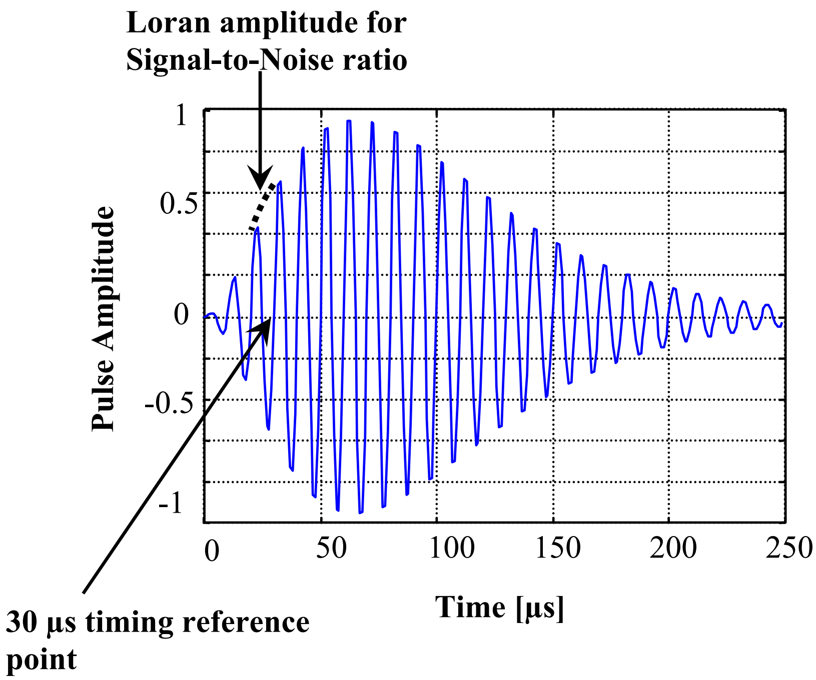

Figure 2.1 Loran-C Pulse Structure

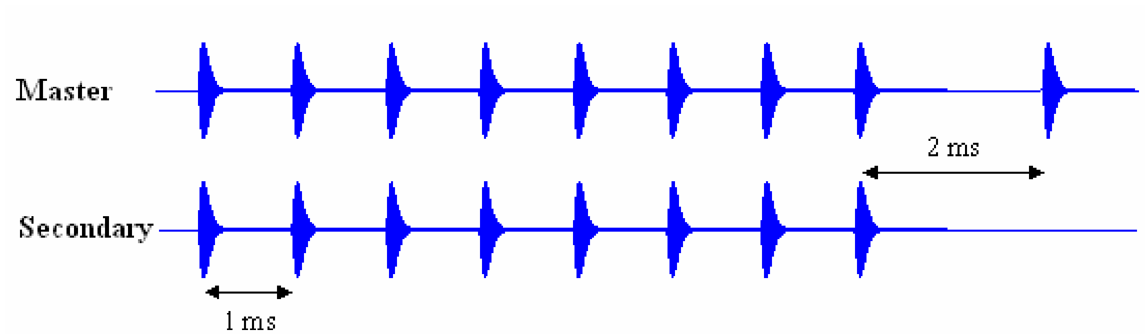

Figure 2.2 Master and Secondary pulse patterns

Some stations have only one function (i.e., to serve as a Master or Secondary in a particular chain), but other transmitters are "dual-rated", meaning that they serve as the Master or Secondary in one chain, and the Secondary for a neighboring chain [1].

Transmitters incorporate Cesium clocks as standard equipment and the timing is synchronized to Universal Time, Coordinated (UTC) to within 100 nsec. The transmitters are monitored by the U.S. Coast Guard, the operator of the system, and associated Loran-C monitor sites are used to detect any anomalous or out-of-tolerance conditions [1].

2.2 Position Determination Using Loran-C

The most often used position determination method for Loran is based on measuring the time difference of arrival (TDOA) of pulses from different stations in a chain to create lines-of-position. In other words, each Master-Secondary pair defines a hyperbolic line-of-position (LOP) based on the time difference (TD) between the reception of Master and Secondary pulses. The intersection of two or more LOPs from the TDs determines the position of the user.

The Master and Secondary stations broadcast radio pulses at precise time intervals. The Secondary stations emit pulse group in alphabetical order of their letter designator after the Master has transmitted its pulse group. For example, consider a simple case of a Master-Secondary pair and a user as shown in Figure 2.3.

The signal transmission is timed as follows: M emits a set of nine pulses. After the M signal reaches W, it delays its transmission for an interval called the Coding Delay (CD). The total elapsed time from the M transmission until the W transmission is termed the Emission Delay (ED) [1]. ED is the sum of propagation time of the signal from M to W plus the CD. The interval between the reception of the Master signal and the W Secondary signal at the user is termed as the TD for the M-W pair.

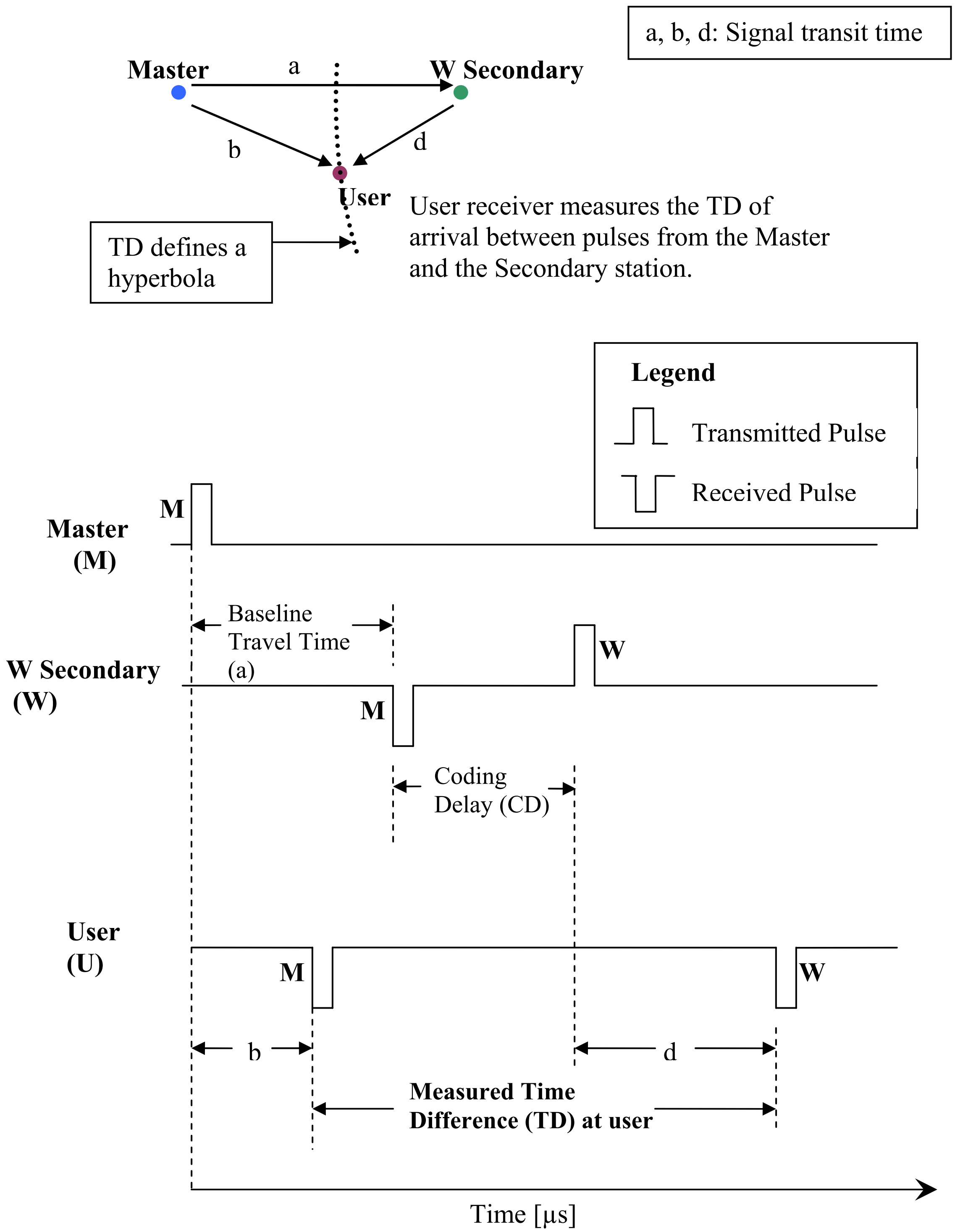

Figure 2.3 Graphical depiction of the Loran-C Time Difference (TD) computation for a Master-Secondary pair

Next, this example is extended to a case with W, X, Y, and Z secondary stations. After W transmits, X transmits a set of eight pulses with a specified CD/ED. Similarly, Y and Z transmit in sequence. The sequence is completed when the Master again starts the transmission of a nine-pulse group [1]. Coding delays are selected such that there are no signal overlaps within a particular chain's coverage region.

For a positioning user of Loran, the receiver position is not known and the TDs for various Master-Secondary pairs are processed to obtain a hyperbolic position fix. The same concept is applied in a reverse way in Chapter 4 to determine the TD between Master-Secondary pairs. With the knowledge of ED, CD and the user and Loran transmitter position information, the TDs for all Master-Secondary pairs can be calculated.

The concept of Loran-C chain timing is illustrated in Figure 2.4 for the North-East U.S. (NEUS) chain.

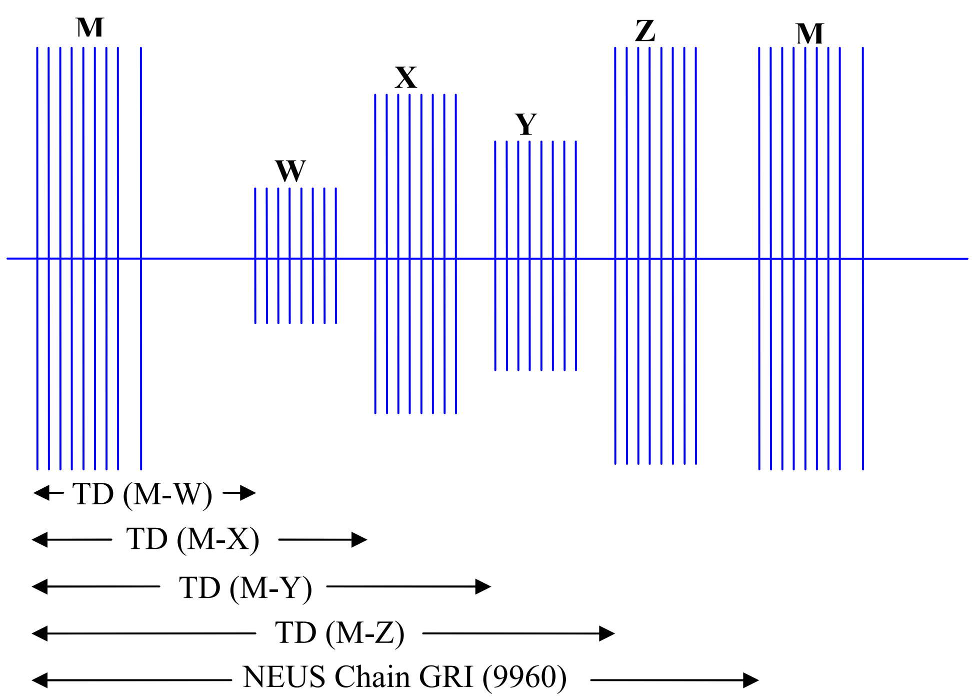

Figure 2.4 Pulse Pattern for the NEUS Chain

The NEUS chain consists of a Master (M) and four Secondary stations (W, X, Y, and Z). Figure 2.4 depicts the North-East U.S. (NEUS) chain (GRI: 9960) that a user in the north-east part of the U.S. might receive. The received signal amplitude of a transmitting station depends on the transmitter power, the distance of the receiver from the station, and the propagation characteristics of the path traveled by the signal.

2.3 Loran-C Propagation

During propagation, the Loran signals broadcast by the transmitters suffer from distortion and interference due to propagation delay variations as a function of terrain, skywave propagation, atmospheric noise, man-made noise, continuous wave interference, cross rate interference, and P-Static.

The speed of propagation of the Loran-C signal depends on the conductivity and permittivity of the surface over which it travels. The speed of propagation of the Loran-C signals must be corrected as a function of the terrain and/or water over which the signal travels. The Primary Phase Factor (PF), Secondary Phase Factor (SF), and Additional Secondary Phase Factor (ASF) account for changes in propagation speed due to air, seawater, and land paths, respectively [1]. Compensation for signal propagation over water is easily accomplished, however, modeling of propagation delays due to different types of soil is fairly complex [6]. Hence, accurate modeling of the ASF values is required for precise navigation and positioning if propagation over land is involved.

There are two paths by which Loran-C signals propagate. The ground wave signals propagate in the atmospheric medium below the ionosphere along the Earth's surface. The Loran-C signals can also propagate as sky waves reflecting from the ionosphere. Sky waves are not desirable for accurate navigation since the propagation conditions in the ionosphere are not stable [1]. Sky-wave contamination can affect the position solution obtained using the Loran-C ground-wave signal.

The source of atmospheric noise is electrical discharges produced by thunderstorms occurring worldwide. Atmospheric noise varies with the time of day, the season, and geographic location.

Man-made noise arises from power transmission, distribution lines, automotive ignition systems, rotating electrical machinery, switching devices, arc generating devices, etc. Man-made noise can be high in urban areas and low in quiet rural locations. Thus, man-made noise (depending on area of operation) can interfere with the Loran-C signals.

In the low frequency (LF) band, there are other communications and navigation systems besides, Loran-C. The interference caused by the near band transmitters is termed as Continuous Wave Interference (CW). This type of interference can be minimized by the use of notch filters.

Stations on different Loran chains transmit at different GRIs. However, all Loran chains share the same frequency band thus resulting in interference from stations with difference rates. This interference is referred to as Cross-Rate Interference (CRI).

Precipitation static (P-static) is caused by aircraft charging during flight through particles of water, snow or dust, which leads to radio noise generated by the electrical discharge from the aircraft or between aircraft components. Aircraft charging can also occur due to engine-produced ionization and electric-cross fields caused by flight below a charged cloud layer. There are three main mechanisms for P-Static [13, 21]:

a) Sparkover or Arcing:

Sparkover or arcing occurs due to potential gradient between different elements of the aircraft. It is mainly due to sparking from an isolated, charged panel to the aircraft structure. Arcs cause pulsed or broadband noise. Proper mechanical bonding of all (isolated) aircraft surfaces can greatly minimize this mechanism.

b) Streamer Currents:

Streamer currents are electrical discharges across non-conducting aircraft parts such as radomes, windshield, and fiberglass panels. The effects of streamer currents are similar to arcs, but conductive coatings may be used to minimize the energy of streamer currents.

c) Corona:

Corona discharge occurs in the presence of ionized air around the trailing edges (wing tips, stabilizers, antenna tips and other protrusions) of an aircraft. This mechanism can be greatly minimized by installing and maintaining static wicks. They are made up of bundles of very fine wire that create an easy path for low-energy discharge for accumulated charge on the airframe.

P-Static can significantly increase the noise level of the received Loran signal, thereby resulting in degraded Signal-to-Noise Ratio (SNR) and loss-of-lock. Anecdotal flight test data show that a loop (H-field) antenna offers significant mitigation to P-static interference compared to a wire (E-field) antenna [15].

The areas of focus of this thesis are atmospheric noise differences between normal and near-thunderstorm flight conditions and a preliminary quantitative investigation into the effects of P-Static noise on wire and loop antennas. Proper modeling of atmospheric noise in the Loran-C band is very important for aviation users, since the effects of lightning discharges may be different for ground and airborne Loran receivers.

Atmospheric noise modeling was initially reported in [10] with the emphasis of the model of navigation systems in the low frequency (30-300 kHz) electromagnetic spectrum. Effects of lightning discharges and its propagation characteristics are provided in [23]. More recently, with the increasing interest in Loran for aviation applications and the formation of the Loran Integrity Performance Panel (LORIPP), noise modeling for the Loran-C band has been an area of research and the subject of several publications [22, 24].

P-Static interference as related to Loran-C is mostly anecdotal. Several publications address P-Static, e.g. [14, 16], while successful mitigation of P-Static has been reported under certain flight test conditions [2, 15]. Because of the promising results from these previous efforts, a detailed data collection and analyses effort was initiated as reported in this thesis. To obtain detailed knowledge of P-Static atmospheric noise in the presence of thunderstorm and associated lightning conditions, a digital flight data collection system was used to sample the entire Loran-C band and to store the data for off-line analyses. The next chapter provides information on the flight test equipment configuration.

3 FLIGHT TEST EQUIPMENT SETUP

This chapter provides a brief overview of the data collection system used for the collection of airborne Loran data. The primary goal of the data collection system is to collect radio frequency (RF) data in the Loran frequency band. In other words, the data collected should provide an accurate representation of the data that would be seen by a Loran receiver.

Figure 3.1 shows the King Air C-90SE that was used for collecting the airborne data.

Figure 3.1 Flight test aircraft (King Air C-90)

Figure 3.2 shows a block diagram of the data collection system installed on the King Air. The data collection PC and the box containing the data collection equipment are mounted in a 19-inch rack (see Figure 3.3) that is installed on the seat rails of the aircraft.

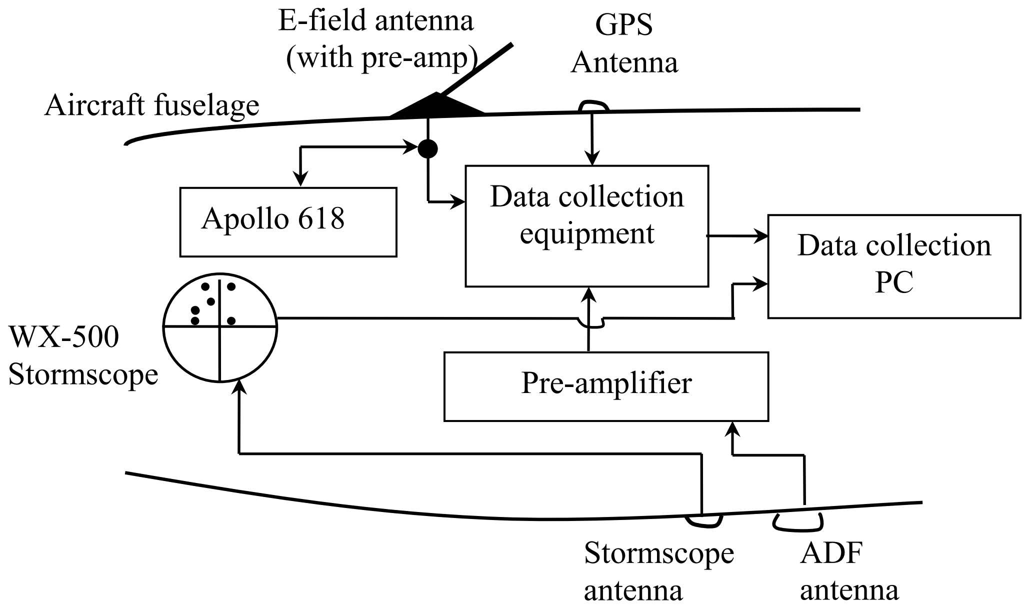

Figure 3.2 Data collection system block diagram

Figure 3.3 Data collection equipment rack

3.1 Equipment Descriptions

This section describes the equipment used in the data collection system.

3.1.1 LORRAD-DS DataGrabber

The LORRAD-DS DataGrabber was developed by Reelektronika, b. v. in The Netherlands. It is designed to collect raw RF data in the Loran band with minimum requirements for external hardware such as filters or amplifiers. The DataGrabber is capable of sampling two antenna input channels simultaneously at 400 kHz with 16 bits of resolution. The dynamic range of the DataGrabber is 96 dB [20]. Figure 3.4 shows the DataGrabber.

Figure 3.4 LORRAD-DS DataGrabber

The data from the DataGrabber are transferred to the data collection PC via an Ethernet connection.

3.1.2 WX-500 StormScope

The StormScope is a part of the aircraft avionics package and it has a range of up to 200 nmi. The StormScope is used for determining the approximate distance of the aircraft from a lightning strike. Lightning strikes are displayed relative to the aircraft heading and the data is output using the RS-232 format at a rate of 9600 Baud [3]. The processing of the StormScope data is outside the scope of this thesis.

3.1.3 NovAtel OEM4 GPS WAAS Receiver

A dual frequency, WAAS enabled OEM4 GPS receiver is used to provide the position and time data during flight-testing. Data is collected from the receiver at a 1 Hz rate using NovAtel's GPSolution software.

3.1.4 Apollo 618 (Loran-C Receiver)

The Apollo 618 (UPS Aviation Technologies) is used to power the antenna pre-amplifier for the E-field antenna. The receiver itself is also used to monitor the Loran-C signals to ensure that the installation is functioning properly.

3.1.5 E-field (Wire) Antenna

The E-field antenna is a II morrow, Inc. (UPS Aviation Technologies), Model A-16 whip antenna with integral pre-amplifier. An Appolo 618 Loran-C receiver powers the pre-amplifier. A picture of the wire antenna mounted on the top of the King Air is shown in Figure 3.5.

3.1.6 H-field (Loop) Antenna

The loop antenna is a King Radio KA 42A Automatic Direction Finding (ADF) Antenna. Figure 3.6 shows the dual-loop antenna installed on the bottom of the King Air. The antenna has two independent loops wrapped around a ferrite block. A custom-built pre-amplifier is used to combine the output of each loop to form an omnidirectional phase pattern (refer [2] for antenna/pre-amplifier details).

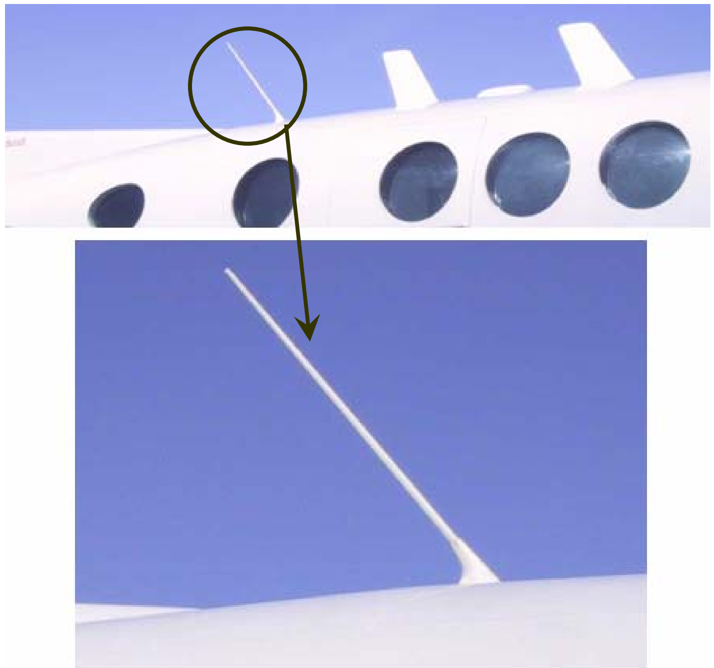

Figure 3.5 Loran-C E-field (Wire) Antenna

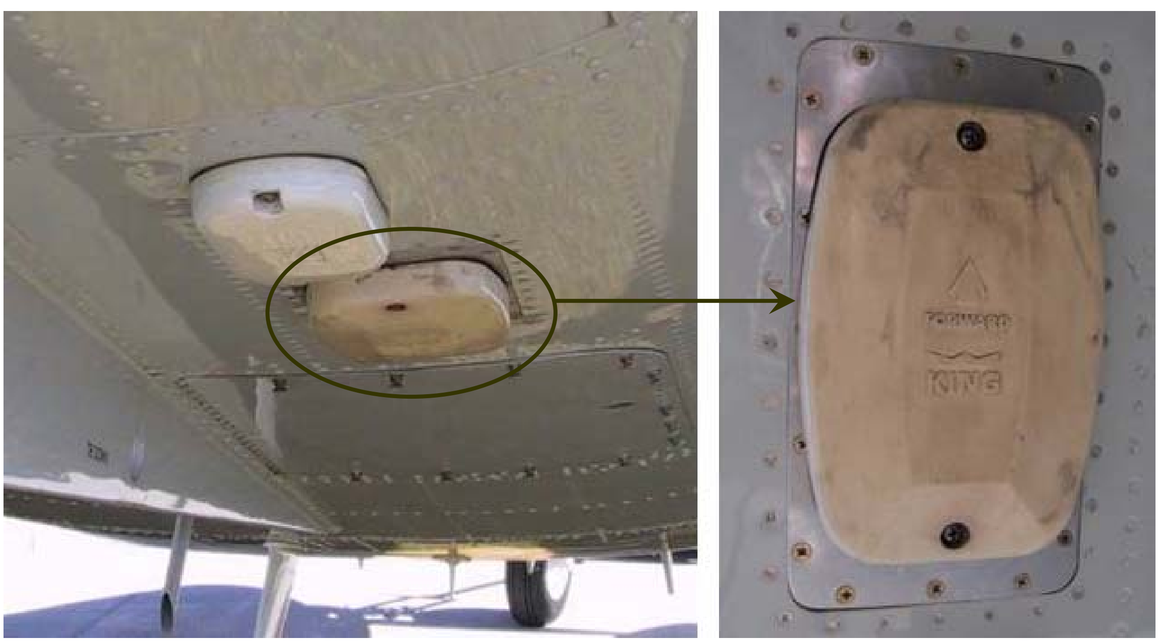

Figure 3.6 Loran-C H-field (Loop) Antenna

3.1.7 Data Collection PC

The data collection computer was manufactured by CyberResearch. It contains two 933 MHz Pentium III single board computers on a dual backplane. These single board computers have the option of supporting Redundant Array of Independent Disks (RAID) arrays on an IDE bus. This feature enhances the capability of the system considering the large amount of data being stored at relatively high rates [3].

For a detailed description of the equipment set-up, the reader is referred to [3].

4 DATA PROCESSING

The data collected using the DataGrabber are processed in 2-second blocks. Figure 4.1 provides an overview of the data processing. The collected RF data are sampled at 400 kSamples/sec and a 2-second data block of the sampled data is used for processing. To characterize atmospheric noise, first, the Narrow-Band (NB) and Continuous Wave (CW) interference present in the signal along with any thunderstorm bursts are removed. Following the removals, the signal consists of the Loran pulses and noise. In order to calculate and characterize the noise, Loran pulses are identified and removed. This is accomplished in the Loran-C processor shown in Figure 4.1.

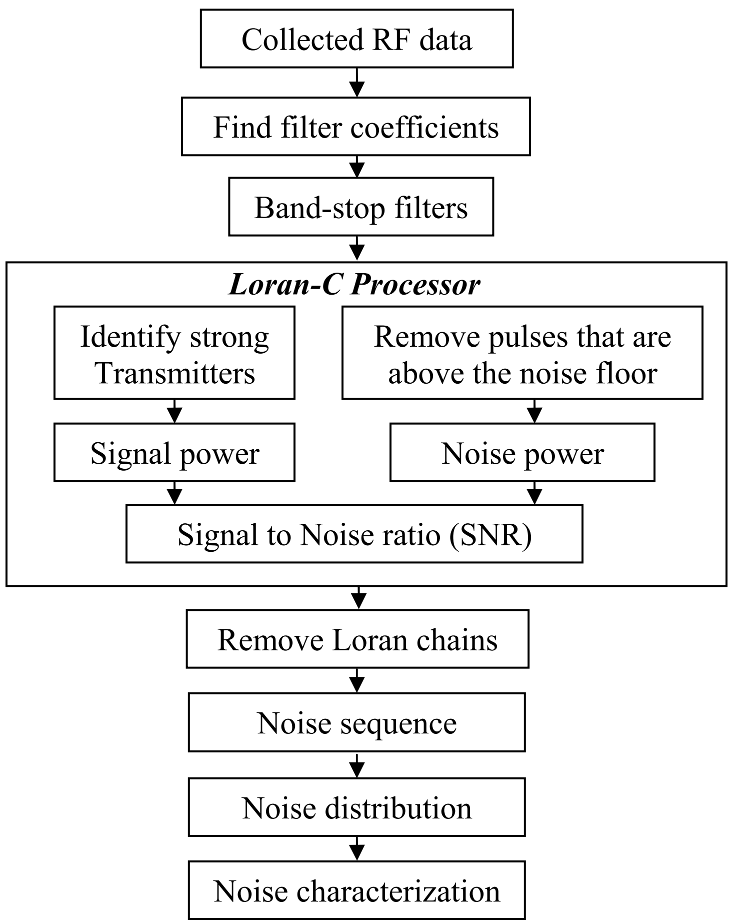

Figure 4.1 Data processing overview

The signal-to-noise ratio (SNR) is computed for transmitters whose signal amplitude is well above the noise floor. The SNR is a function of user location as well as atmospheric noise. SNR in this thesis is calculated as the SNR value measured at the output of the antenna. It is noted that this SNR is not the same as the SNR of the signal in space, since at the output of the antenna, antenna gain and pre-amplifier noise figure modify the SNR. In this thesis, no conclusions are derived from the SNR, but the values are included to verify the proper functioning of the data collection system and the processing algorithms.

Figure 4.2 shows the detailed diagram of the data processing. CW and NB interference detection is performed by passing the signal through a bank of band-pass filters, each with a bandwidth of 500 Hz, and squaring the output of the filters. After identifying a potential interference source from the first 2-second data block, the filter coefficients are calculated and stored for the subsequent 2-second data blocks. Using the filter coefficients, the CW and NB interferences are filtered from the signal using bandstop filters.

Thunderstorm bursts have a high energy level compared to the noise floor. To remove noise bursts caused by such inclement weather conditions, the signal energy is calculated in time-bins and a time-bin is discarded if the bin has energy above a set threshold. At this point in the processing, the signal contains Loran-C pulses and noise. The signal is integrated over the PCI of the Loran chain and the stations with signal amplitude above the noise floor are identified using the known user position. Note that the thunderstorm-induced noise burst that are removed from the data are retained for later analyses.

Samples that contain Loran-C pulses are removed. The remaining noise sequence is used to characterize the noise and to calculate the noise distribution.

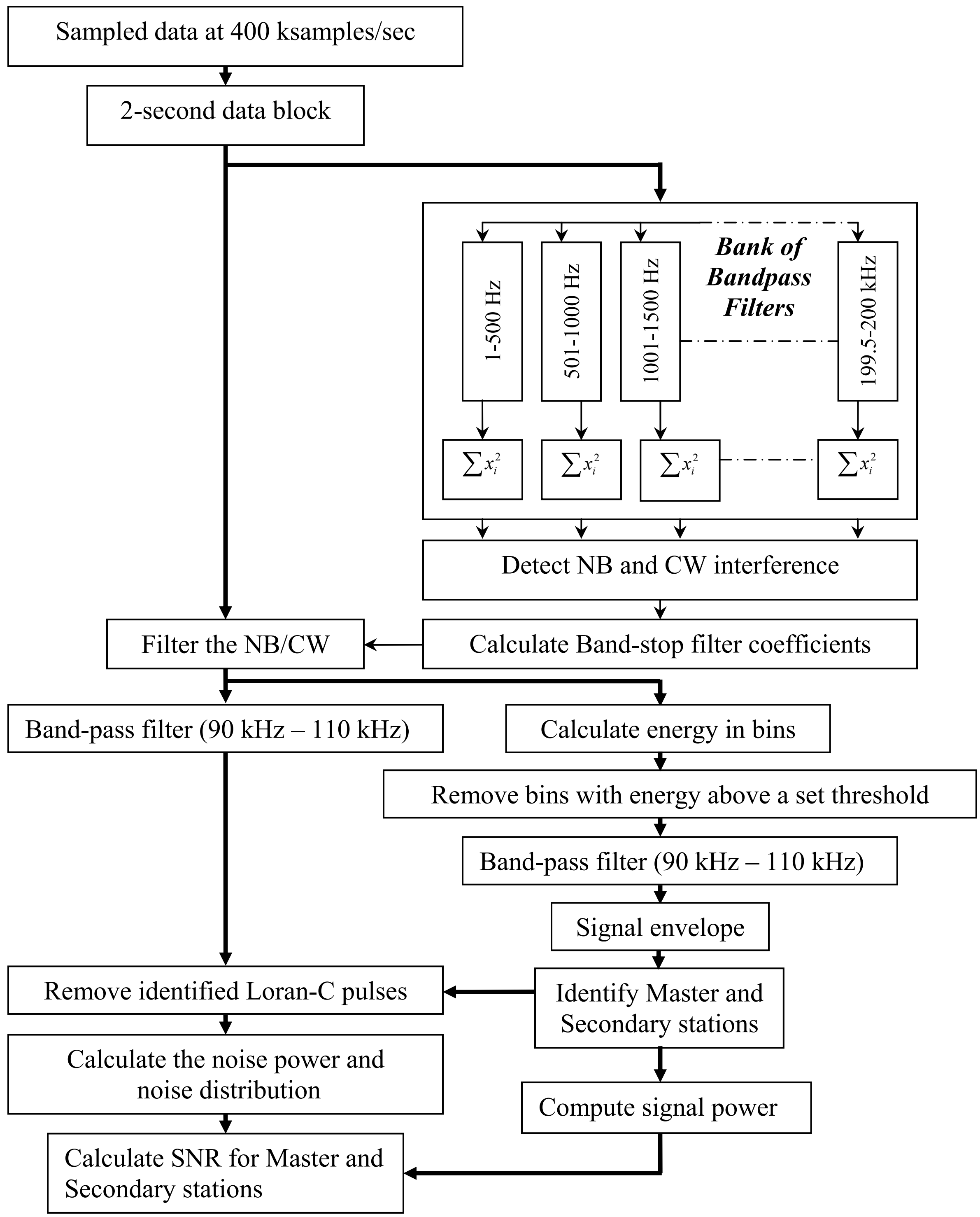

Figure 4.2 Data Processing

4.1 Detection of NB and CW interference

The 2-second data block is passed through a bank of band-pass filters, each with a bandwidth of 500 Hz. Thus, 400 such filters are used to detect the NB/CW around the center frequency of 100 kHz. Using a smooth curve fit as the reference, frequency-bins that contain NB/CW are identified and removed using a band-stop filter. The signal is then band-pass filtered using a second order Butterworth filter with a center frequency of 100 kHz and pass-band from 90-110 kHz. The signal obtained at the end of this step is used to characterize atmospheric noise after removing the Loran pulses. To remove the Loran pulses, the chains must be identified; this is described in sections 4.2 through 4.6.

4.2 Detection and Removal of Thunderstorm Bursts

During thunderstorm activity, the Loran-C signal can be affected by the lightning discharge of the thunderstorm. The noise bursts must be removed for identification of Loran chains and calculation of signal strength. For detection of the thunderstorm bursts, the 2-second data block is divided in bins and signal energy is calculated in time-bins as follows:

$$\text{Energy in a bin} = \sum_{i=1}^{N} (x_i)^2 \tag{4.1}$$

where:

N = number of samples in each bin

x_i = amplitude in A/D levels of i^{th} sample

Length of each bin is 5-ms thus resulting in 400 bins in a 2-second data block. Energy in every bin is calculated and the average energy of 400 bins multiplied by a factor (user defined) is used as a threshold for bin removal for a particular 2-second data block. If the energy in any bin is above this threshold value then, that bin is filled with zeros, thus removing the thunderstorm bursts.

4.3 Identification of Loran Chains

The signal available after removal of the NB/CW interferences and thunderstorm bursts consists of the Loran pulses and noise. This signal is band-pass filtered for the Loran Band (90-110 kHz) using a second order Butterworth filter with a center frequency of 100 kHz. The filtered signal is then down-converted to baseband and the sum frequency terms are removed using a second order Butterworth low-pass filter with a cut-off frequency of 50 kHz. The envelope of the signal is formed using in-phase (I) and quadrature-phase (Q) components. Next, the envelope is used for the identification of the Loran chains and to calculate the signal strength of strong, received signals. This method of downconverting and using the I and Q component overcomes the problem of undersampling and enables proper reconstruction of the signal [12].

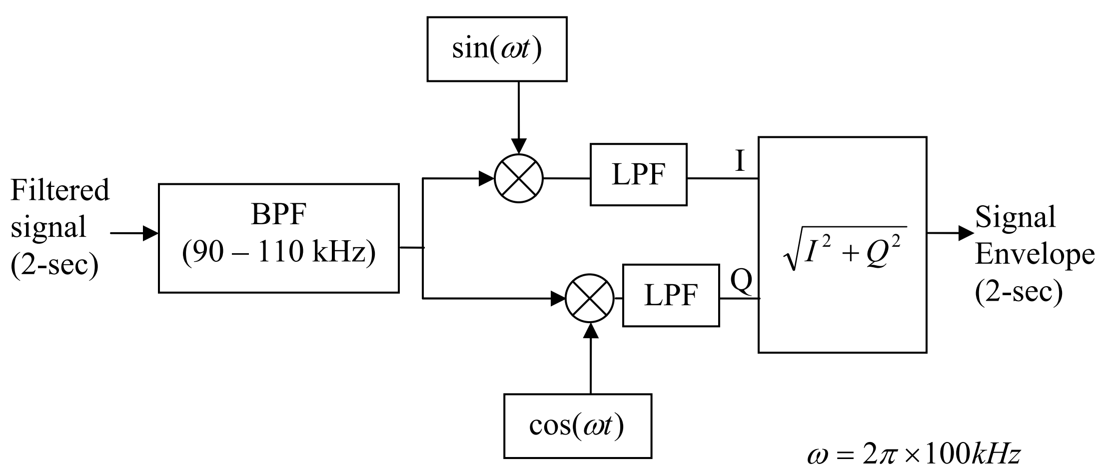

Figure 4.3 Extraction of the signal envelope from the filtered signal

The 2-second signal envelope is then divided into sequences (blocks) of PCI length (for respective chain). For example, the NEUS chain with a GRI of 99600 μs (PCI of 199200 μs) has 10 whole PCI blocks. When the blocks are added, the pulse groups of the PCI of interest will amplify while, the other PCIs (or chains) are attenuated. The block addition is limited to 2 seconds due to oscillator drift and unkown antenna motion. In the remainder of the thesis, this will be referred to as integrating PCIs.

An example of unprocessed 2-second data block for the H-field antenna channel is illustrated in Figure 4.4. The data used here were collected during a flight test on August 13, 2003 near Akron, Ohio. Signal amplitudes are expressed in A/D levels, which can range between -32767 to +32768.

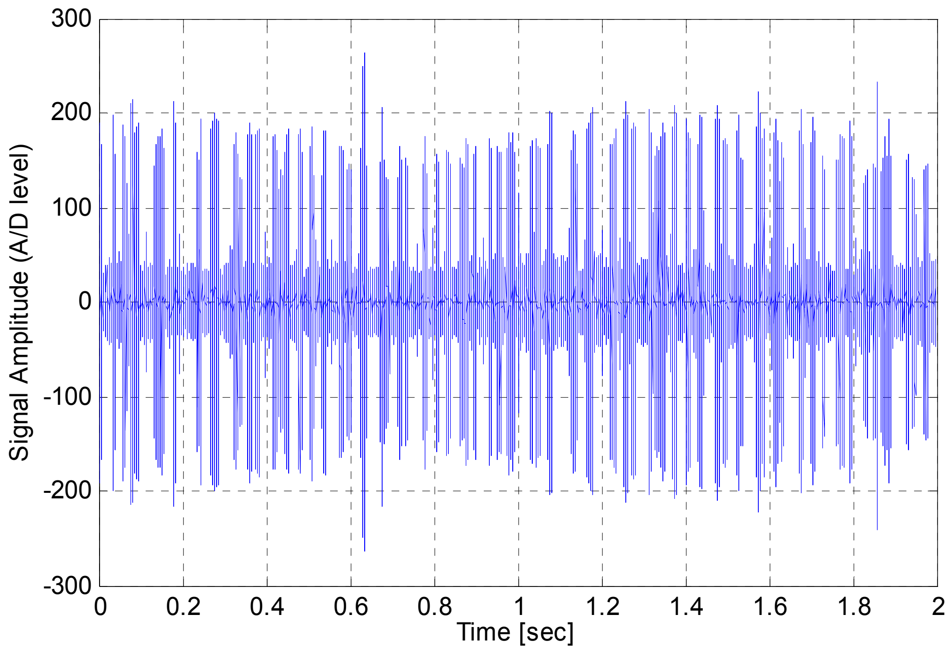

Figure 4.4 H-field antenna channel unprocessed 2-second data block

After extraction of the I and Q components from the 2-second data block, the signal envelope is obtained as depicted in Figure 4.5.

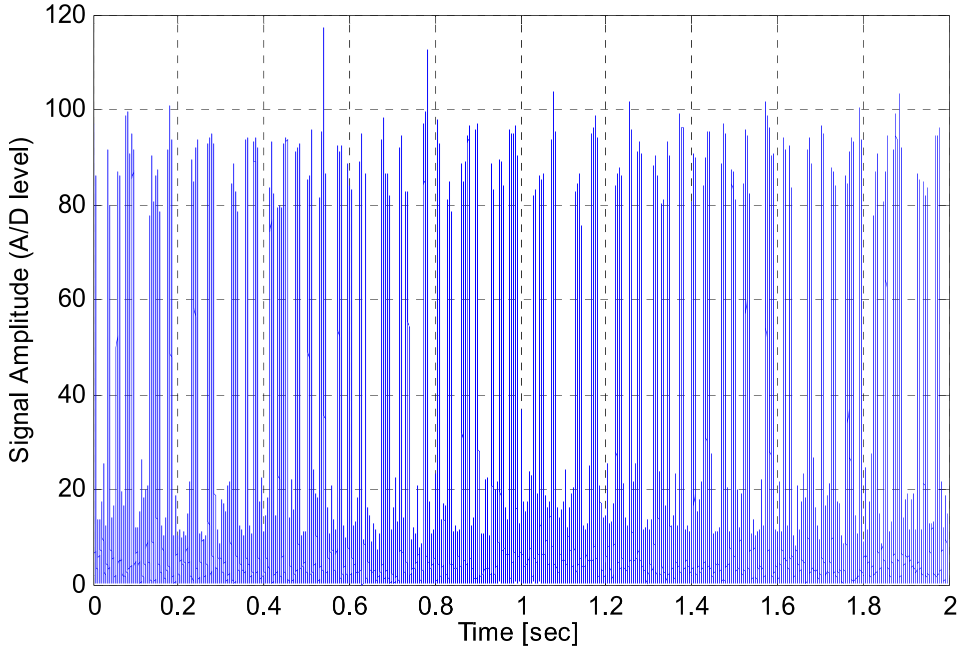

Figure 4.5 Two-second signal envelope for an H-field antenna channel

After the block addition for the PCIs of the NEUS chain, the Master and the Secondary stations for the NEUS chain can be clearly seen in Figure 4.6.

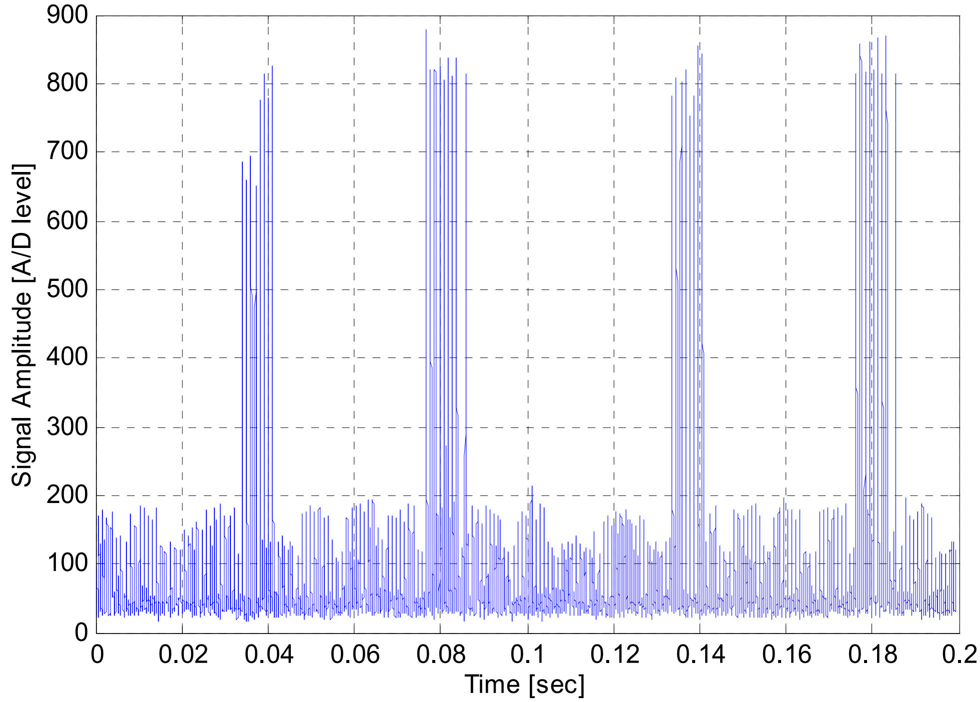

Figure 4.6 H-field antenna channel after integrating PCIs for the NEUS chain

The transmitter for the Master station of the NEUS chain is located in Seneca, New York. The locations of the Secondary stations can only be determined after proper identification of each Secondary transmitter. This is accomplished by using the GPS position information, the coding delay and the emission delay as explained in Section 2.2. The next step is to obtain the exact sample number of the first pulse of the Master and each Secondary which will be used in calculating the signal strength.

A flowchart for identification of a loran chain is shown in Figure 4.7. Prior to the Master station identification, a group of nine pulses, a threshold for the noise floor is set to make the tracking process faster.

The difference in time between peaks of two successive pulses is 1 millisecond (or 400 samples). This timing relationship is used to search for groups of eight pulses. For example, in Figure 4.6, if a signal amplitude threshold of 200 is set, then, four groups of eight pulses are found. The Master pulses consists of nine pulses with the ninth pulse spaced two (or 800 samples) milliseconds from the eighth pulse. This property is used to identify the master.

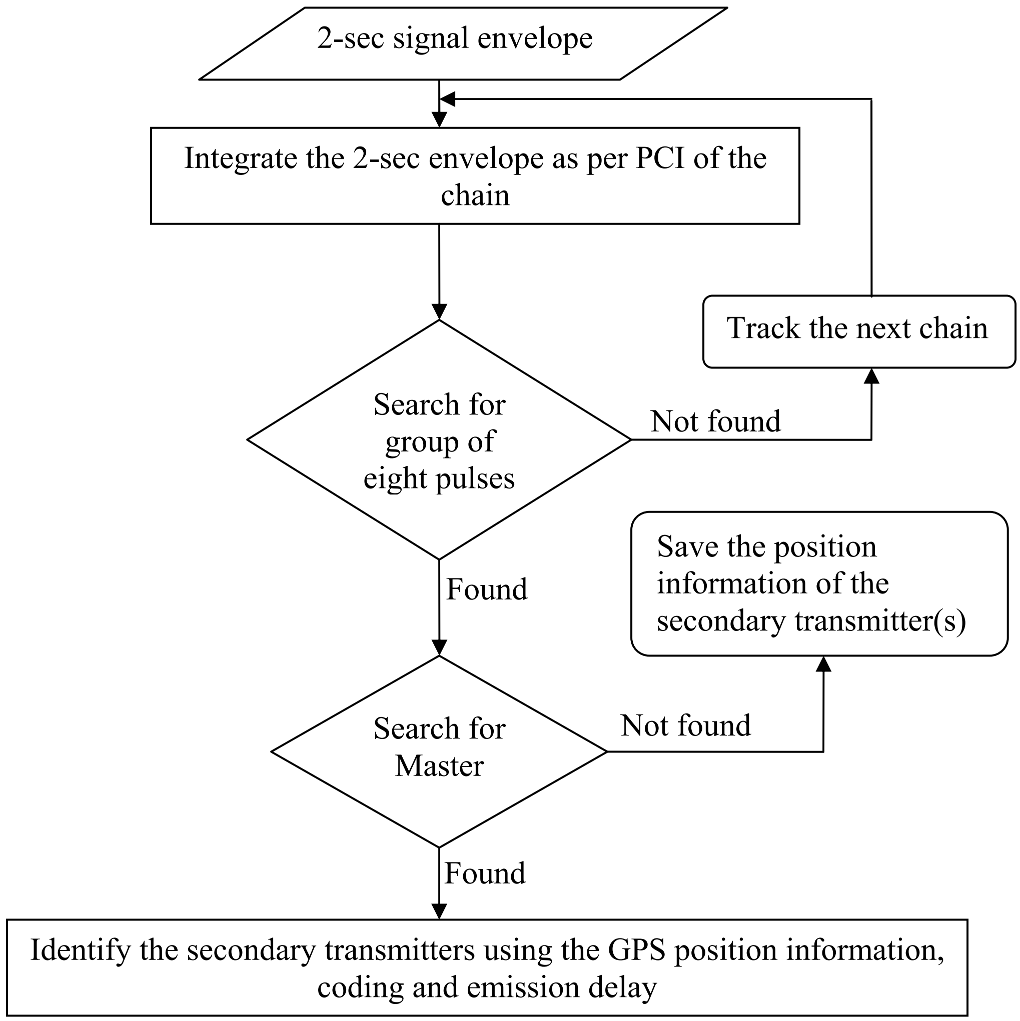

Figure 4.7 Identification of a Loran Chain

After a Master station is identified, the sample spacing between the Master and Secondary is calculated. This information along with the GPS position information, coding delay and the emission delay is used to identify the Secondary. For example, using this identification logic, the Secondary transmitter shown in Figure 4.6 is identified as the Z station located at Dana, Indiana. Figure 4.8 shows the identified stations for the NEUS chain.

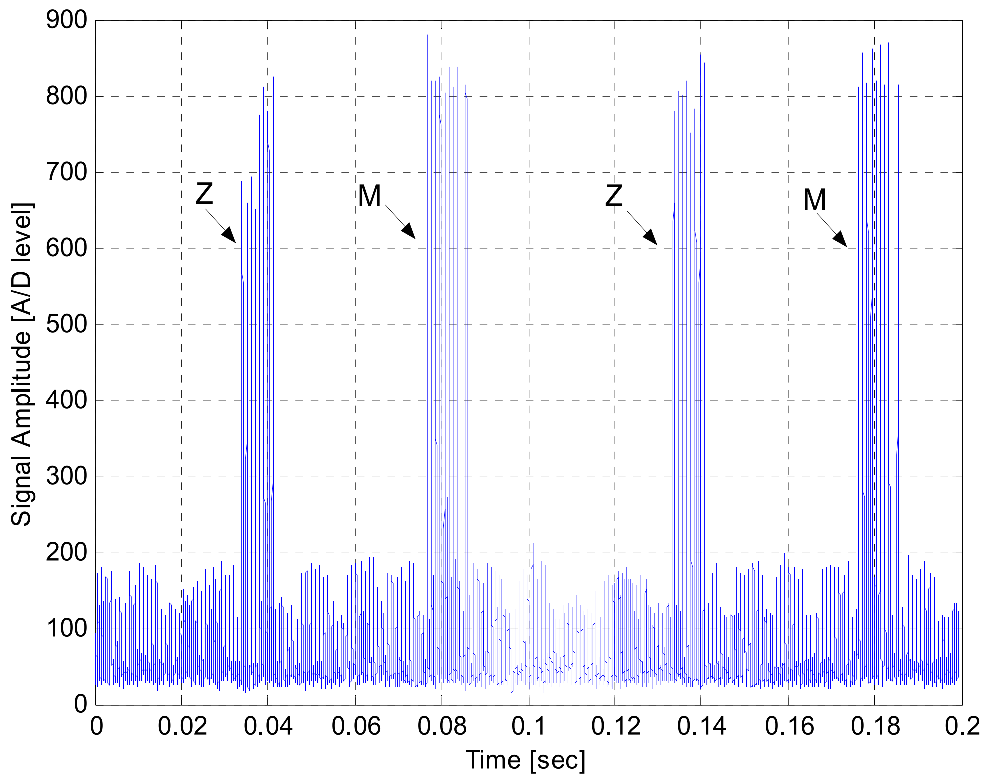

Figure 4.8 H-field antenna channel after integrating PCIs and tracking for the NEUS chain

In the processing software, identification is implemented for all chains in the continental U.S., and all chains in Canada, Alaska and Europe.

4.4 Signal Strength Calculation

Signal strength is calculated for the stations that are well above the noise floor. Since block addition of PCIs is implemented, the added block consists of a pair of Master and Secondary transmitting stations. Prior to calculating the signal strength, the signal strength of both the Masters (and both the Secondary stations) is compared. If the ratio of signal strengths is less than 95% then, signal strength of both the Masters (and Secondary stations) for every PCI is calculated. A PCI with signal strength ratio less than 93% of two Masters (or Secondary stations) is declared as a bad PCI for that particular PCI of Master (or Secondary). If the number of bad PCIs exceed a certain number, then the 2-second data block is ignored and the signal strength is set to zero. However, the 2-second data block is used for calculating the noise distribution.

The amplitude of the envelope at 25-μs is used for calculating the signal strength. After successful identification, the starting point of the first pulse of the Master (or Secondary) is known. However, successive pulses of the Master (or Secondary) are not always 1-ms (or 400 samples apart). To ensure the accuracy of the signal strength calculation, relative spacing of every pulse of the Master (or Secondary) is calculated and if it is within a certain set threshold then the signal strength of the pulse is computed (see Figure 4.9).

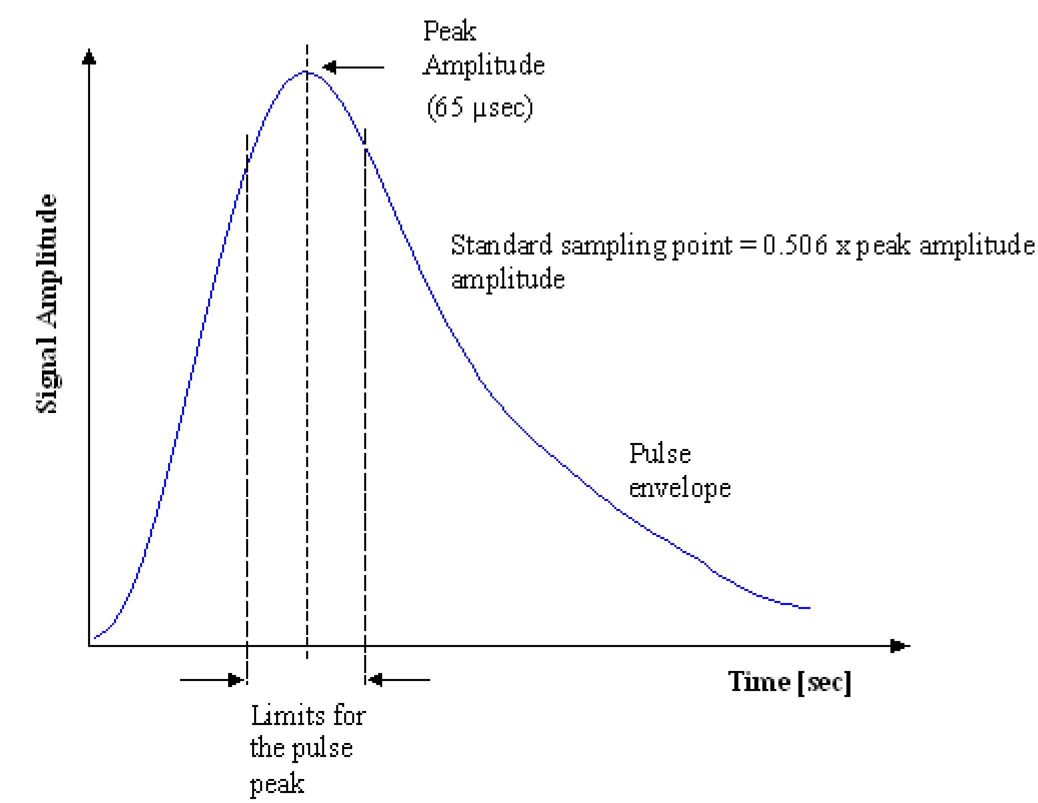

Figure 4.9 Signal strength calculations

If the timing information exceeds the set threshold then, that pulse is ignored. Thus, pulses affected by interference, skywave or noise are excluded from the signal strength calculations.

The Root Mean Square (RMS) value of the pulse is calculated by using:

$$\text{RMS value} = \sqrt{(0.506 \times peak\ amplitude)^2} \tag{4.2}$$

The RMS value of every good pulse is calculated and that value is used in calculating the signal strength for each transmitter. For example, if all nine pulses of a Master station are good, then the signal strength of the master station is given by:

$$\text{Signal strength} = \frac{Average\ of\ rms\ value\ of\ nine\ pulses}{Number\ of\ PCIs\ added} \tag{4.3}$$

4.5 Calculation of the rms value of noise

The next step in the processing involves removal of the identified Loran pulses. Consider Figure 4.8 as an example, wherein the Master and the Z Secondary are identified. By using the known Secondary station locations, the known user location from GPS, and the known CDs and EDs, the pulses from the Secondaries can be approximated in relation to those from the Master. The location of the Secondary pulses are subsequently removed from the data. Similarly, Loran signals transmitted by other chains (whose Masters are identified) are removed.

For chains whose Master is not identified but there is one or more Secondary stations well above the noise floor, the position information of the Secondary stations is used to remove the Loran signals (see figure 4.7).

After the removal of all identified Loran pulses, only a noise sequence is left, as shown in Figure 4.10. The extreme left and right portions of the noise sequence is intentionally filled with zeros to take care of the leftover pulses from the previous and the next 2-second data blocks.

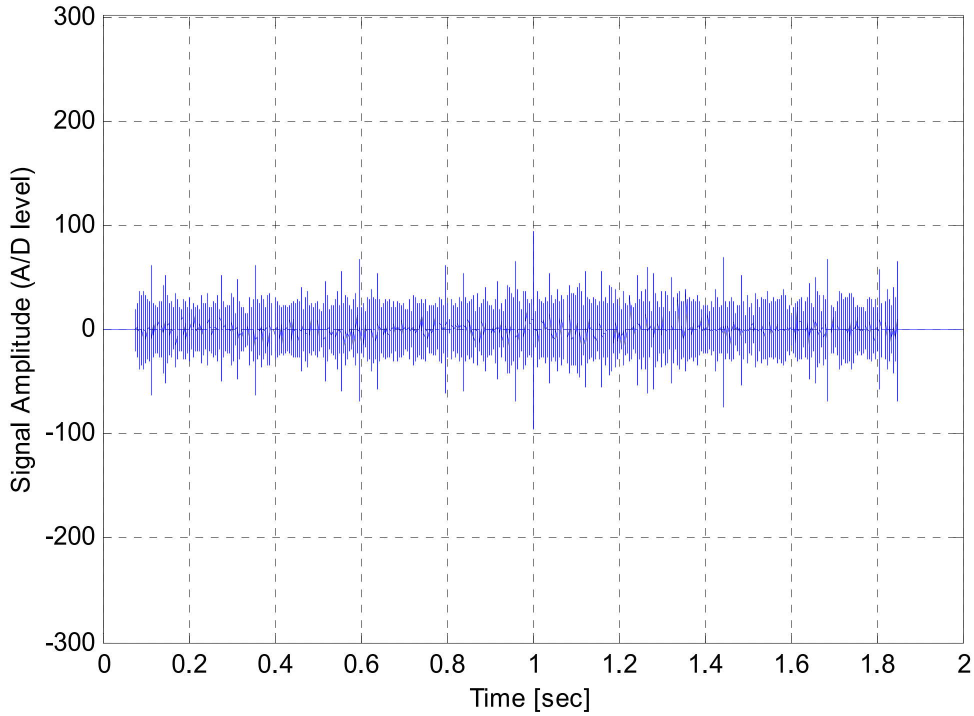

Figure 4.10 H-field antenna channel after removal of Loran pulses

Note that all the identified Loran-C pulses are removed. In this example, it includes all the Secondary stations from the NEUS and Great Lakes chains and the pulses from the SEUS chain.

The RMS value of noise is calculated for samples that have non-zero amplitude within the -10σ to 10σ range. An estimated value of σ is set prior to processing.

The RMS value is calculated as follows:

$$\text{Noise RMS} = \sqrt{\frac{\sum_{i=1}^{N} x_i^2}{N}} \qquad (4.4)$$

where:

x_i = Amplitude of the ith non-zero sample

N = number of non-zero samples

The signal-to-noise ratio (SNR) for the 2-second data block is computed using the calculated signal strength of the transmitter and the rms value of noise.

$$\text{SNR} = 20\log_{10}\left(\frac{Signal\ Strength}{Noise\ RMS}\right) \qquad (4.5)$$

4.6 Characterization of atmospheric noise

The SNR computation is performed for every 2-second data block and the distribution of the noise sequence is accumulated and plotted at the end of the data set. The average value of noise RMS is calculated for the entire data set and used for plotting the Gaussian cdf as explained in the next paragraph.

After all the data blocks are processed, the distribution of the noise samples is plotted and used for calculating the cumulative distribution functions (cdf and 1.0 - cdf). For comparison of this cdf with the Gaussian cdf, a Gaussian cdf with a value of the calculated σ is plotted against the calculated cdf on a log scale.

The Gaussian cdf is plotted in MATLAB using the built-in Complementary Error function (erfc) using:

$$y = 1 - 0.5erfc\left(x/\sqrt{2}\right) \quad \text{for } \sigma = 1 \qquad (4.6)$$

where:

$$\text{erfc(a)} = \frac{2}{\sqrt{\pi}}\int_{a}^{\infty} e^{-t^2}\,dt = 1 - \text{erf(a)}$$

Thus, the noise statistics involve comparing the calculated cdf of noise and the Gaussian cdf with the same standard deviation as the noise.

This completes the processing algorithms. The same processing is implemented for the E-field as well as the H-field data sets. The results obtained for different weather conditions using the processing software are discussed in chapter 5 through 7.

5 FLIGHT TEST I (NORMAL CONDITIONS)

This section describes the results obtained from the first flight experiment; the flight was flown under normal conditions in Ohio. Flight data near Columbus, Ohio were collected on August 13, 2003 from 09:00:08 to 09:05:32 local time. Figure 5.1 illustrates the trajectory obtained using the GPS receiver. The airborne data were collected at an ellipsoidal height of approximately 4 km.

Figure 5.1 First flight test trajectory

Since the North-East U.S. (NEUS) chain provided better coverage than any other chain for the given flight trajectory, SNR values for the NEUS chain transmitters were calculated. The Master station (located in Seneca, NY) and the Z Secondary (located in Dana, IN) provided good signal strengths, and hence, SNRs were calculated for these stations. Figure 5.2 shows the Loran-C transmitter locations in the NEUS chain.

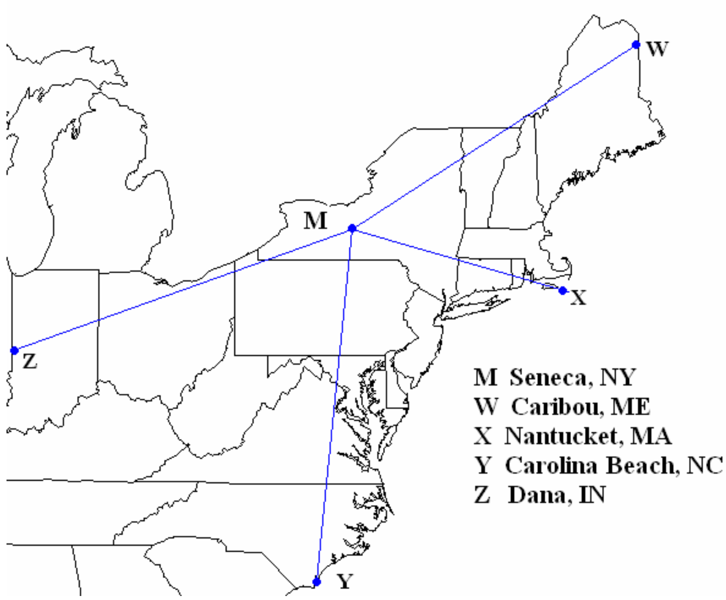

Figure 5.2 North-East U.S. Loran-C Chain

A Multiplication factor of 5.2 is used for removal of thunderstorm bursts (as explained in section 4.2) for the E-field and the H-field data. This factor was set after considering the noise floor of the data and was found to be an effective value for removing thunderstorm bursts. Since this data was collected under normal conditions and was not affected by thunderstorm bursts the threshold was never reached.

5.1 E-field Antenna Channel Results for First Flight Test

Results obtained using the E-field antenna channel are described in this section. Figure 5.3 shows a 2-second portion of the raw data collected from the E-field antenna channel. The Loran pulses visible in the figure are mainly from the NEUS chain, Great Lakes (GL) chain and South East U.S. (SEUS) chain.

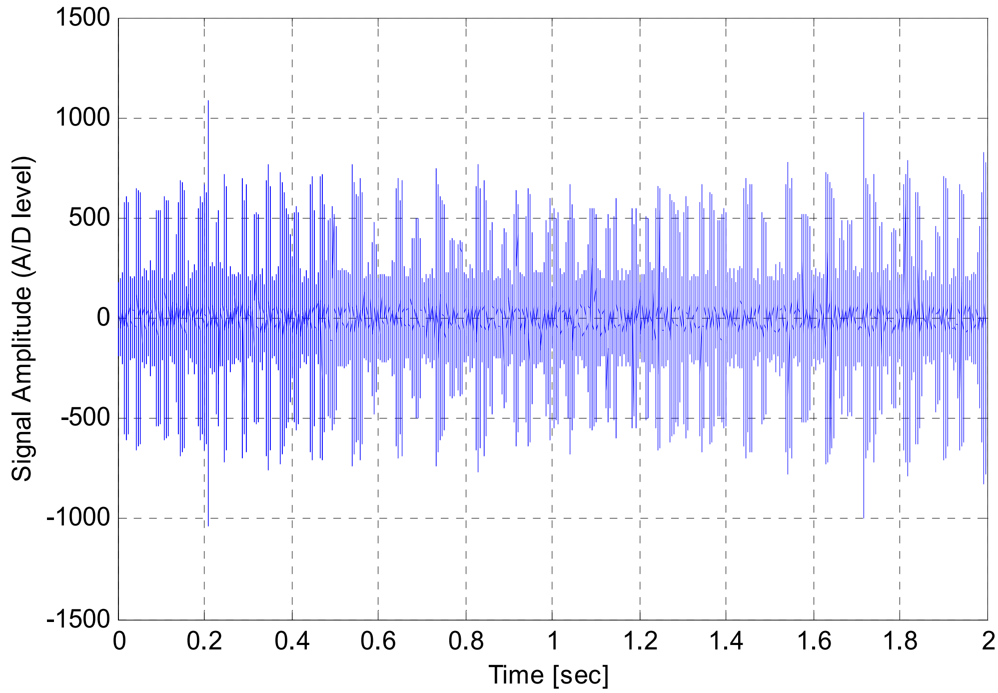

Figure 5.3 E-field antenna channel unprocessed 2-second data block for the first flight test

After filtering, down converting and extracting the I and Q signals from the raw signal as explained in Chapter 4, the signal envelope is obtained as shown in Figure 5.4.

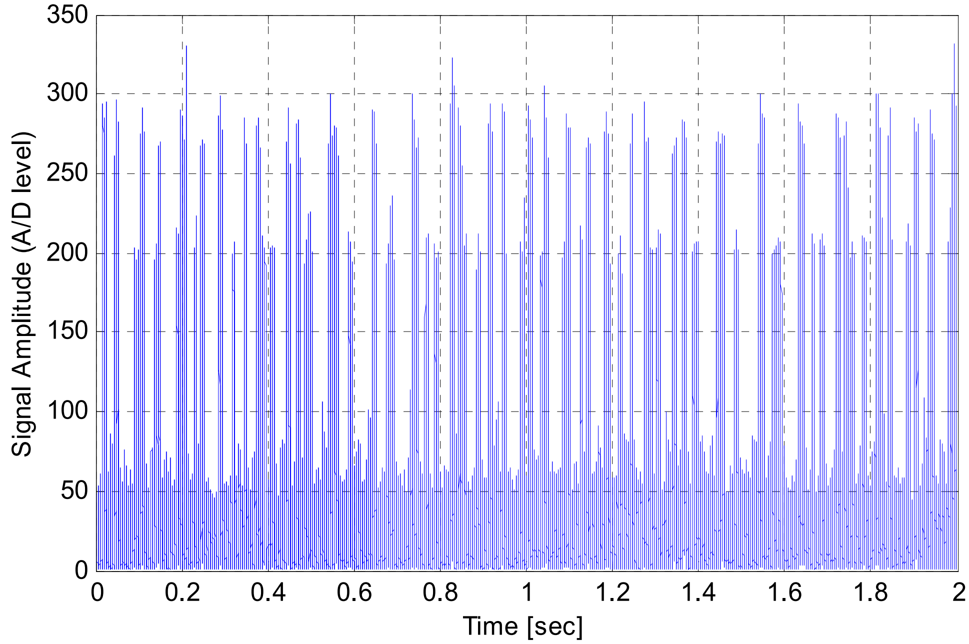

Figure 5.4 E-field antenna channel signal envelope for the first flight test

After integrating the PCIs for the NEUS chain, two occurrences of the Master and two occurrences of the Z Secondary are visible in Figure 5.5. Signals from Y Secondary (located in Carolina Beach, NC) are visible too in Figure 5.5 however, its signal strength is relatively low compared to the Master and the Z Secondary and therefore, only the SNR values of M and Z are computed.

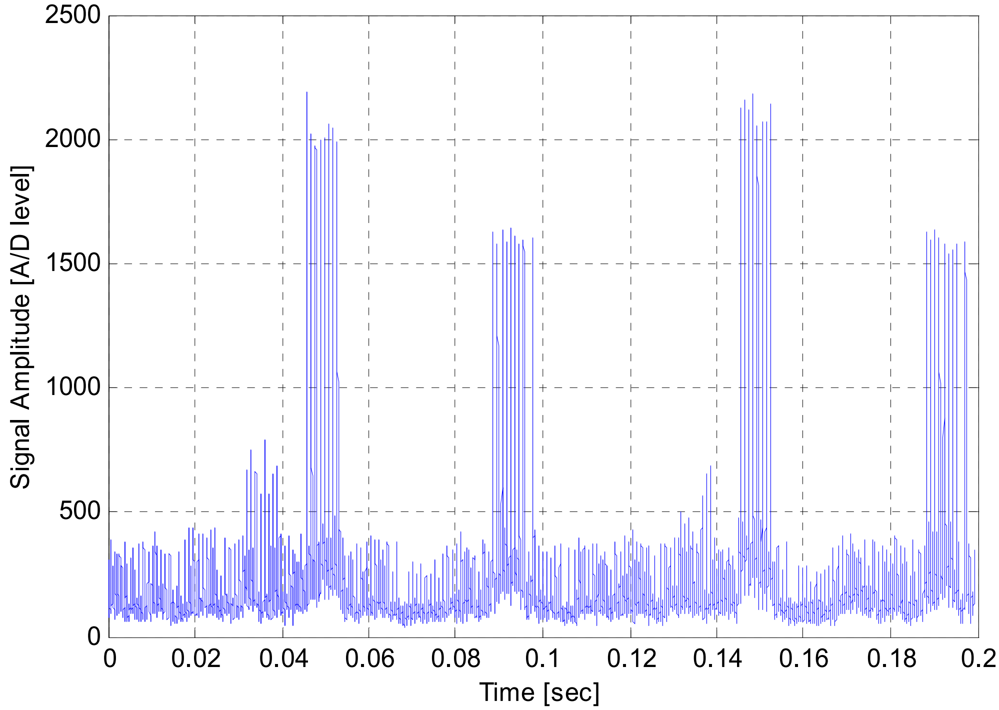

Figure 5.5 E-field antenna channel data after integrating the PCIs for the NEUS chain for the first flight test

Loran-C transmitter locations in the GL chain are shown in Figure 5.6. After integrating the PCIs for the GL chain, occurrence of a Master and a Secondary can be seen in Figure 5.7. The Master station for the GL chain is located in Dana, IN and the Secondary is X-ray (X) located in Seneca, NY. Since the signal strengths of W (located in Malone, FL), Y (located in Baudette, MN) and Z (located in Boise City, OK) Secondary stations are low; it is difficult to identify them in Figure 5.7.

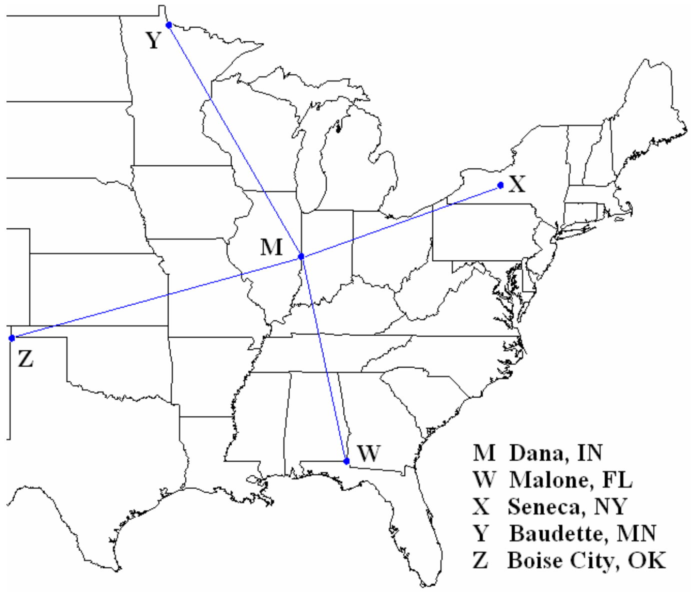

Figure 5.6 Great Lakes Loran-C chain

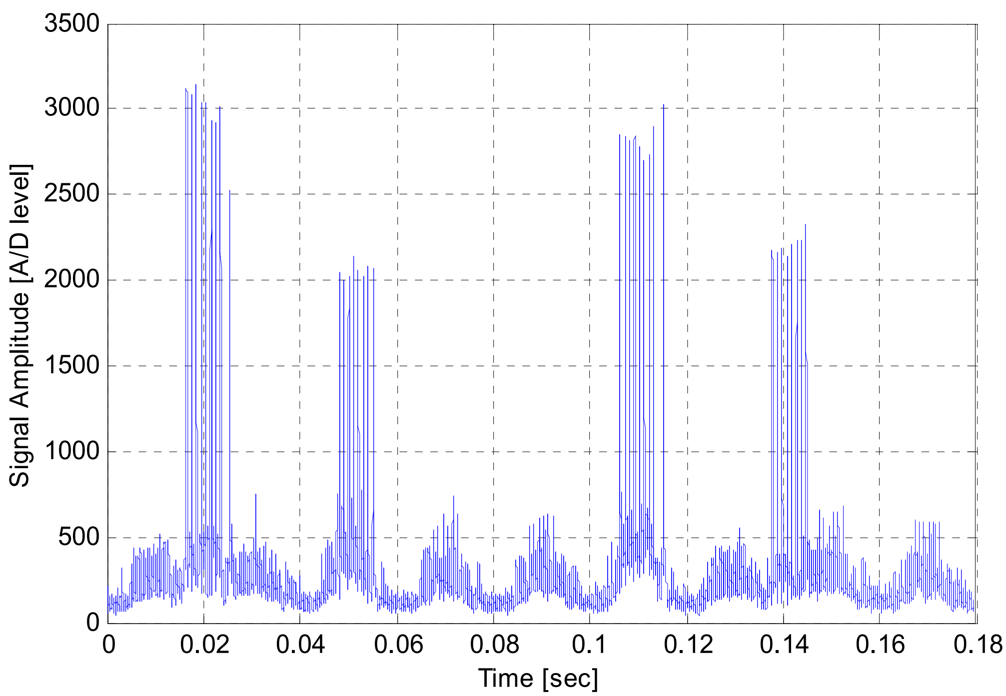

Figure 5.7 E-field antenna channel data after integrating the PCIs for the GL chain for the first flight test

Figure 5.8 shows the E-field antenna channel data after integrating the PCIs for the SEUS chain. Since the SEUS chain coverage is mostly in the southern part of the U.S., no significant signal strength of any station is visible. However, occurrence of a Secondary station can be seen in Figure 5.8. Since there is no Master visible, the Secondary station cannot be identified. However, the position information of the Secondary station is used for removal of pulses while calculating the noise floor as explained in Chapter 4.

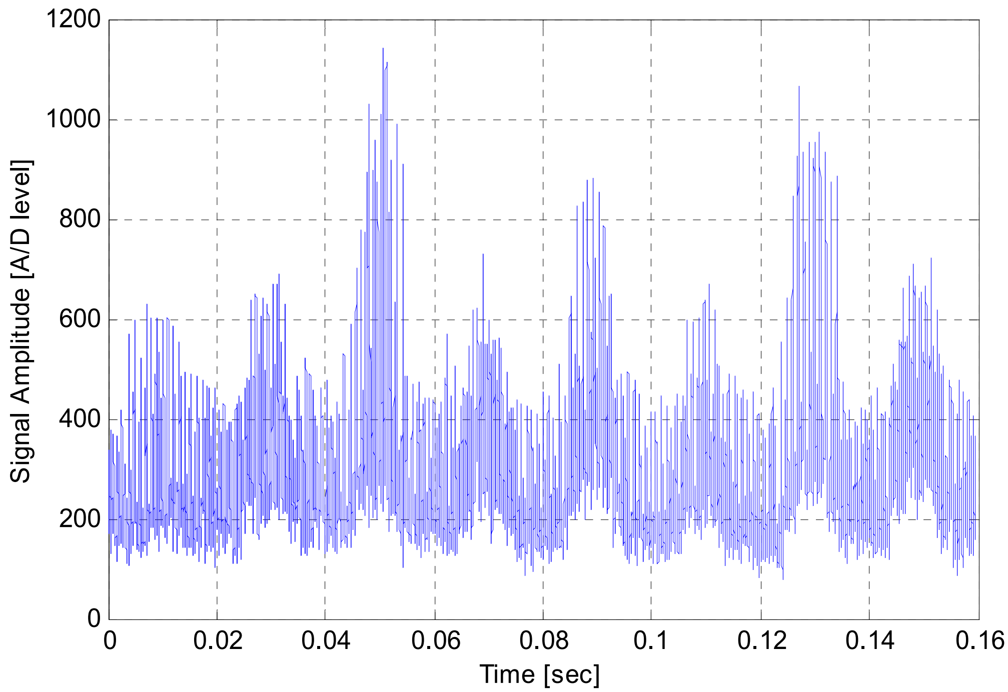

Figure 5.8 E-field antenna channel data after integrating the PCIs for the SEUS chain for the first flight test

Similarly, the PCIs are integrated for other Loran chains and the identified stations are removed to calculate the noise sequence. The top plot in Figure 5.9 shows the unprocessed signal before removal of the Loran pulses, while the bottom plot shows the noise sequence after removal of the Loran pulses.

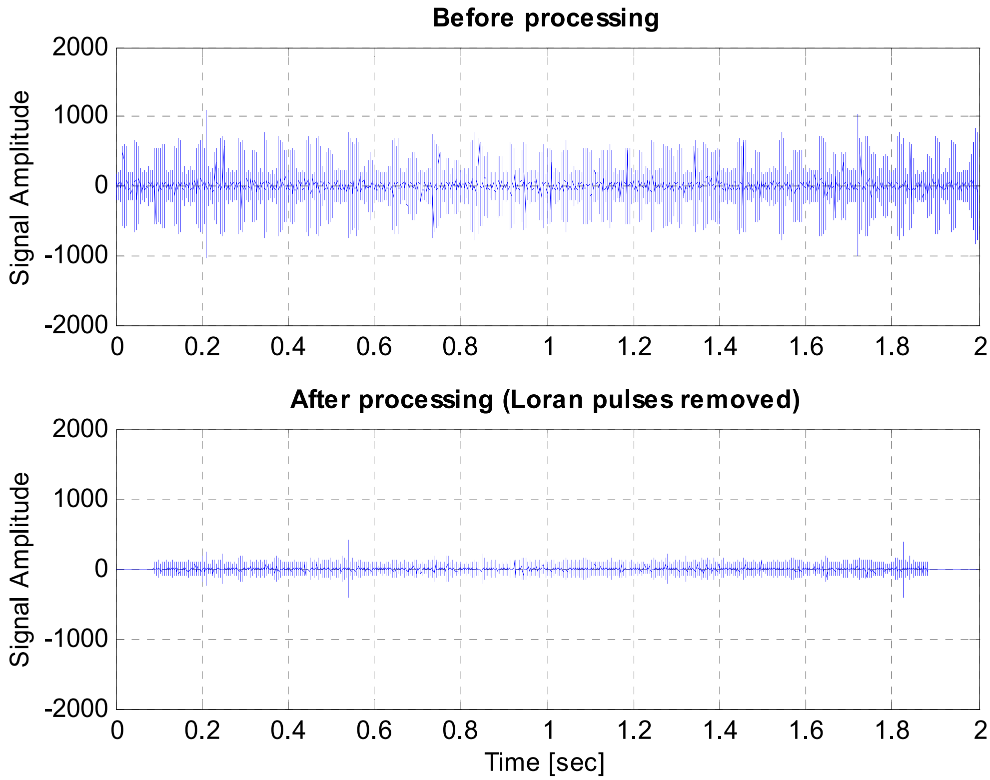

Figure 5.9 E-field antenna channel before (top-plot) and after (bottom plot) removal of Loran pulses for the first flight test

The entire data set is processed in a similar way and the calculated RMS values of the Master, Z Secondary, and noise for every 2-second data block is plotted. Figure 5.10 shows such plot for the entire 326-second (2×163) data set. The noise floor was fairly stable throughout the data set.

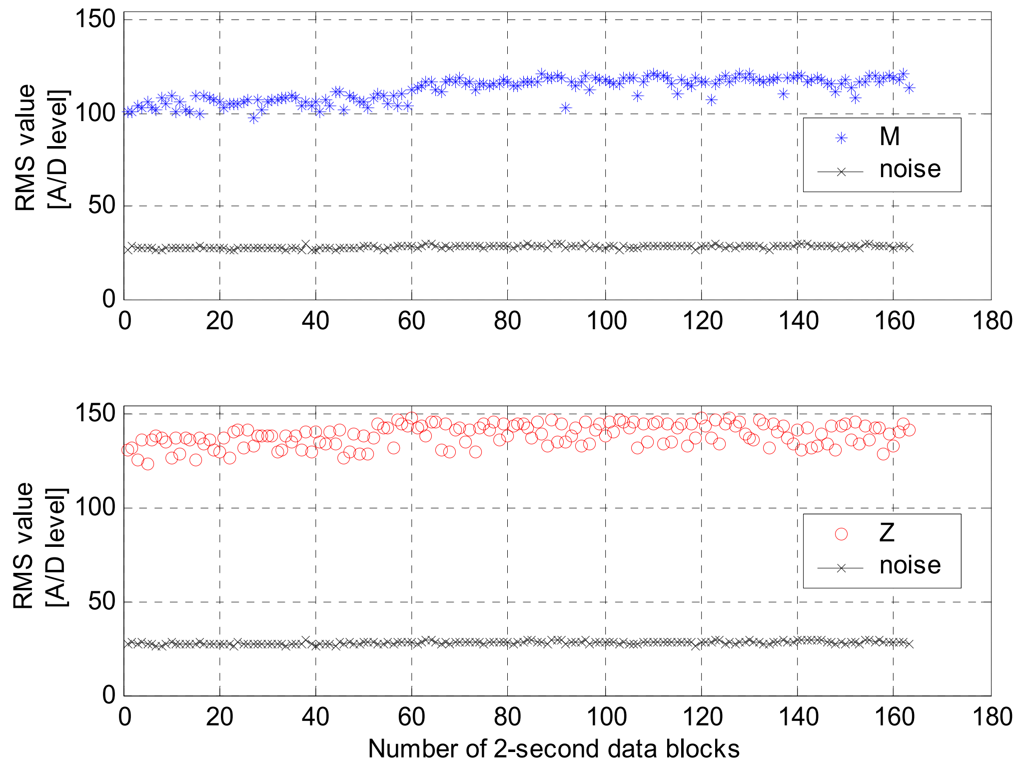

Figure 5.10 E-field antenna channel RMS values for Master, Z secondary (NEUS chain) and noise for the first flight test

Next, the distribution of the noise samples for the entire 326-seconds data set (approximately 130 million samples) is computed and plotted in Figure 5.11. This distribution provide experimental data for probabilities as small as 10^{-7} (see Figure 5.12).

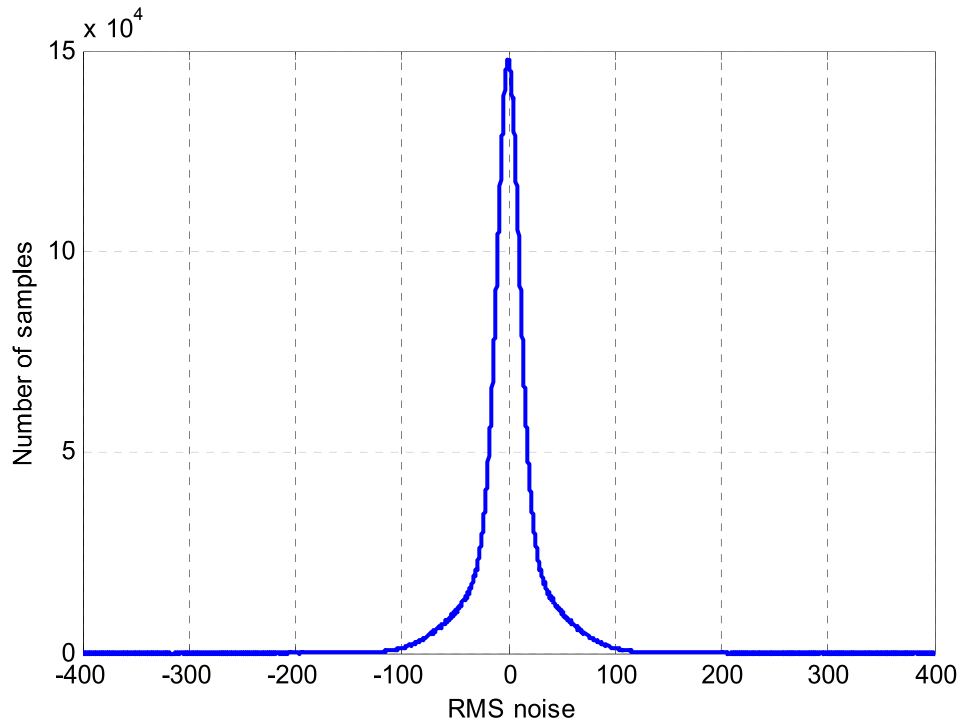

Figure 5.11 E-field antenna channel noise distribution for the first flight test

From the noise distribution, the cumulative distribution functions (cdf and 1.0 - cdf) of the noise is calculated and plotted against the Gaussian cdf (with the same standard deviation as the noise) in Figure 5.12. The plot indicates that the tail probabilities of the calculated noise cdf (and 1.0 - cdf) are larger than the Gaussian cdf (and 1.0 - cdf) with an equivalent rms value. Noise of the collected data can be overbounded by a Gaussian distribution that has three times the standard deviation of the collected noise. Overbounding means that the probability of exceeding a certain noise realization is less than the corresponding probability of a Gaussian realization.

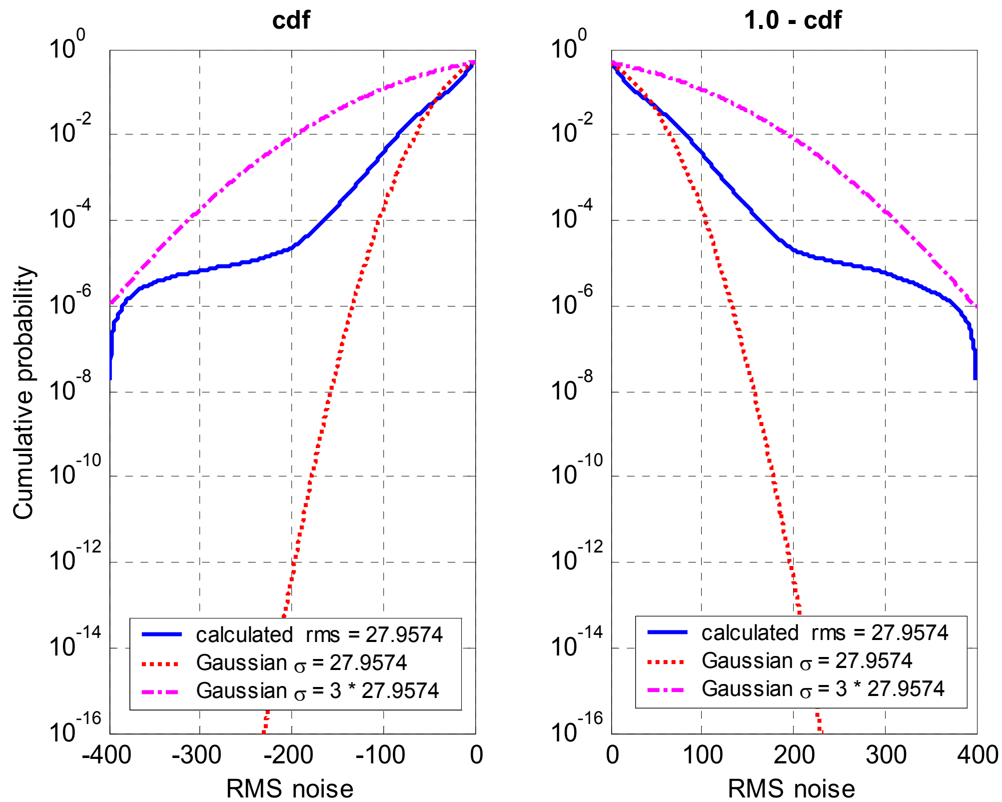

Figure 5.12 E-field antenna channel noise statistics for the first flight test

5.2 H-field Antenna Channel Results for First Flight Test

The data collected from the H-field antenna is processed in a similar way as those for the E-field antenna. Figure 5.13 shows an unprocessed 2-second data block collected using the H-field antenna. The H-field antenna path has a lower overall gain compared to that of the E-field antenna path. Therefore, the signal amplitude at the output of the H-field antenna is lower when compared to the E-field antenna output. For these tests, equal amplitudes for the E-field and the H-field signals were not necessary for the comparison of the performance of the two antenna systems. The 2-second signal envelope obtained after filtering and downconversion is shown in Figure 5.14. This signal is integrated over the PCIs for the NEUS chain and the result is shown in Figure 5.15.

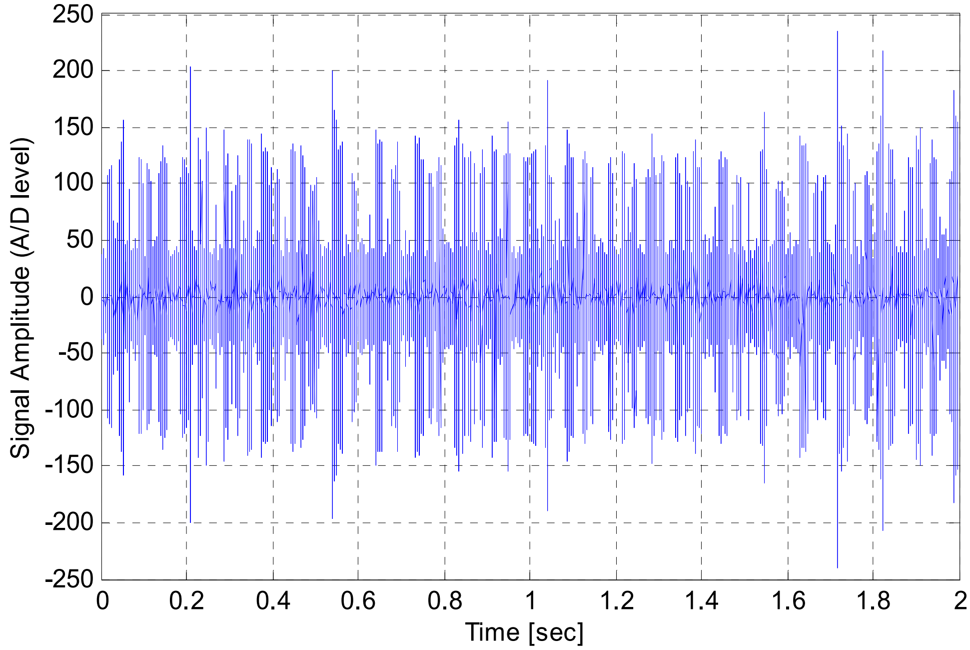

Figure 5.13 H-field antenna channel unprocessed 2-second data block for the first flight test

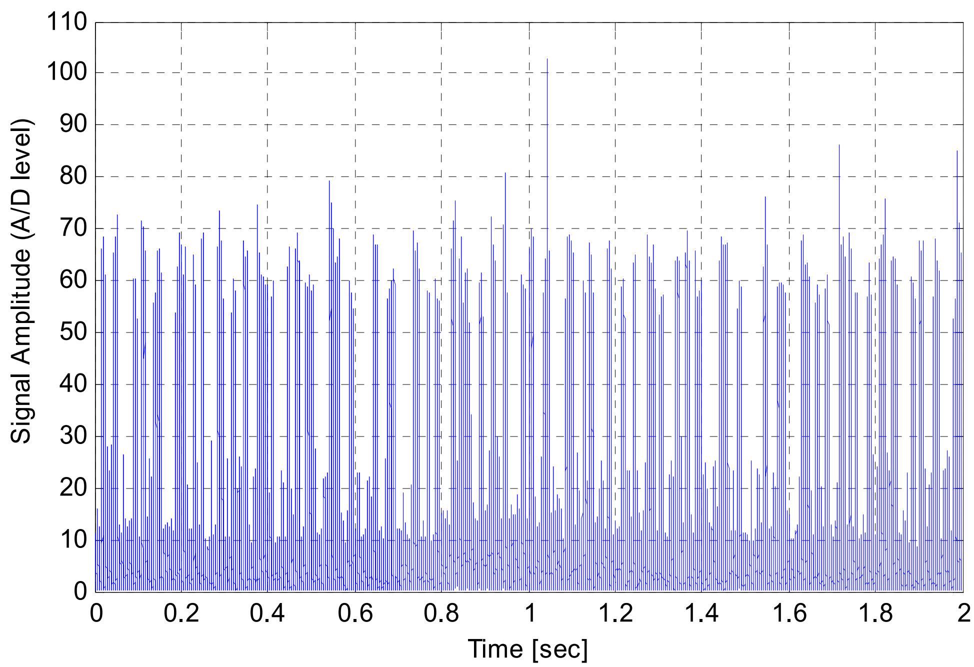

Figure 5.14 H-field antenna channel signal envelope for the first flight test

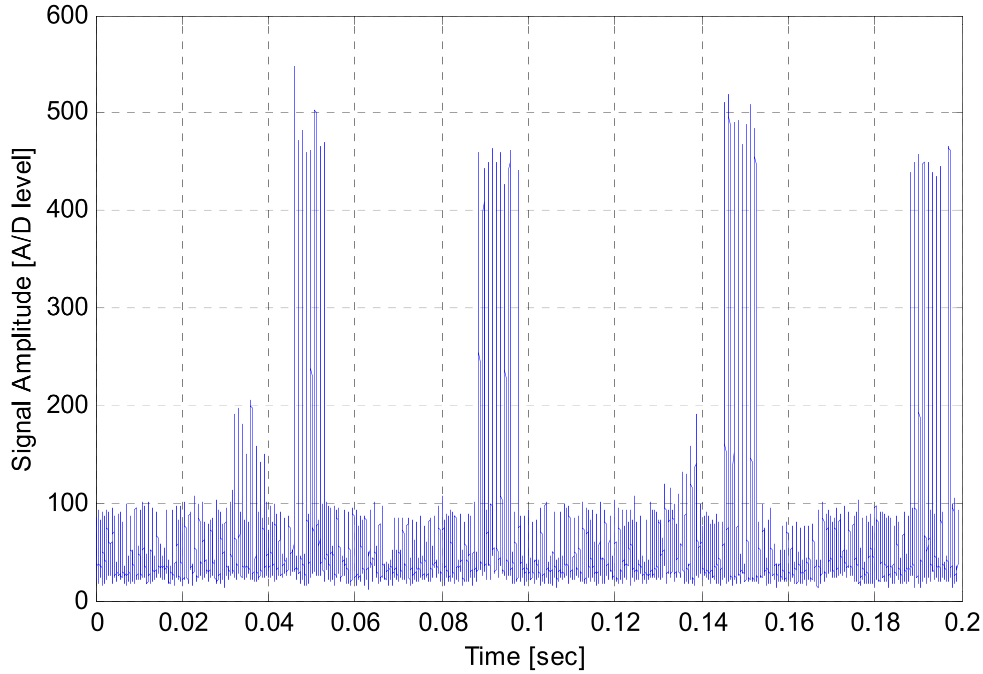

Figure 5.15 H-field antenna channel data after integrating the PCIs for the NEUS chain for the first flight test

Similar to Figure 5.5, after integrating the PCIs for the NEUS chain, two occurrences of the master and two occurrences of the Z secondary are visible in Figure 5.15.

Similarly, after integrating the PCIs for the GL chain, the occurrence of a Master and a Secondary can be observed in Figure 5.16. The results obtained here are identical to the E-field data discussed in the previous section. The Master station and the X Secondary for the GL chain have good signal strength near Columbus, Ohio due to the proximity of the stations. Presence of W, Y and Z Secondary signals can be seen in Figure 5.16, but due to the weak signal strength, the amplitudes of these stations is close to the noise floor. For the H-field data too, multiplying factor of 5.2 is used for removal of thunderstorm bursts (as explained in section 4.2).

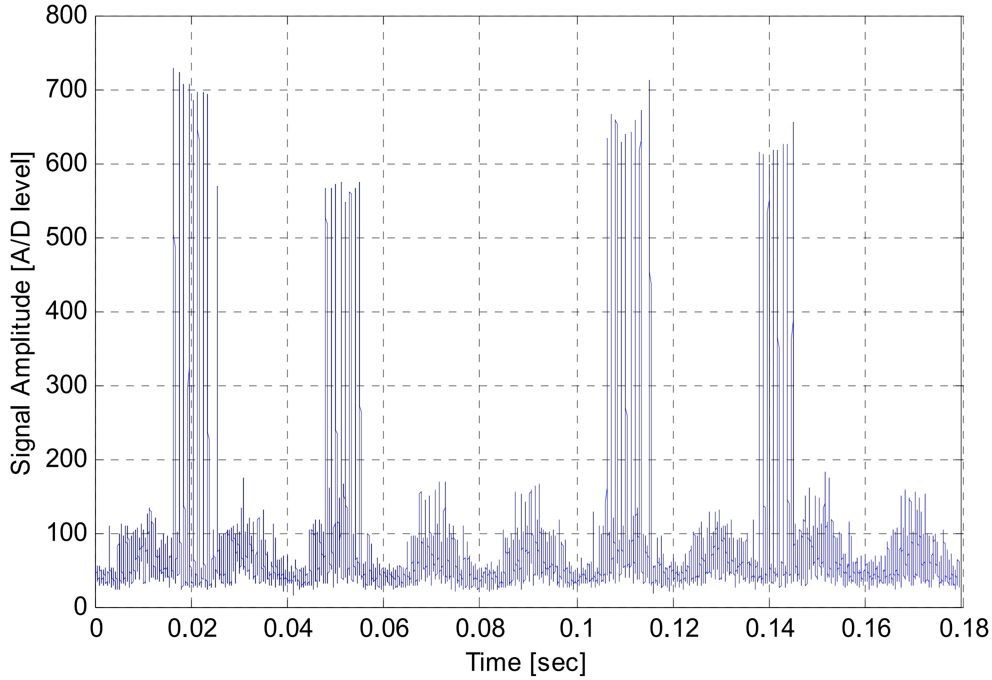

Figure 5.16 H-field antenna channel data after integrating the PCIs for the GL chain for the first flight test

Figure 5.17 shows the signal obtained after integrating over the PCI for the SEUS chain. As mentioned previously, the chain coverage of the SEUS chain is mostly in the southern part of the U.S., so, no significant signal strength of any station is visible near Columbus, Ohio. However, occurrences of a Secondary station can be seen in Figure 5.17. Since there is no Master visible the secondary station cannot be identified. However, the position information of the Secondary station is used for removal of pulses while calculating the noise floor as explained in Chapter 4.

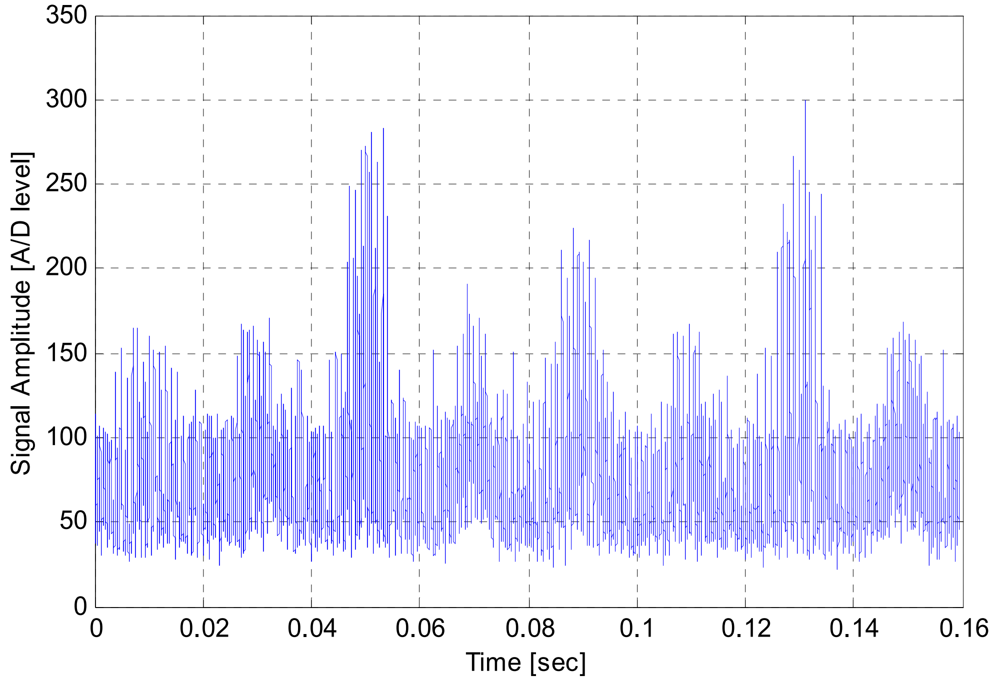

Figure 5.17 H-field antenna channel data after integrating the PCIs for the SEUS chain for the first flight test

The top plot of Figure 5.18 shows the unprocessed 2-second data block, while the bottom plot shows the noise sequence after removal of the Loran pulses for the H-field antenna.

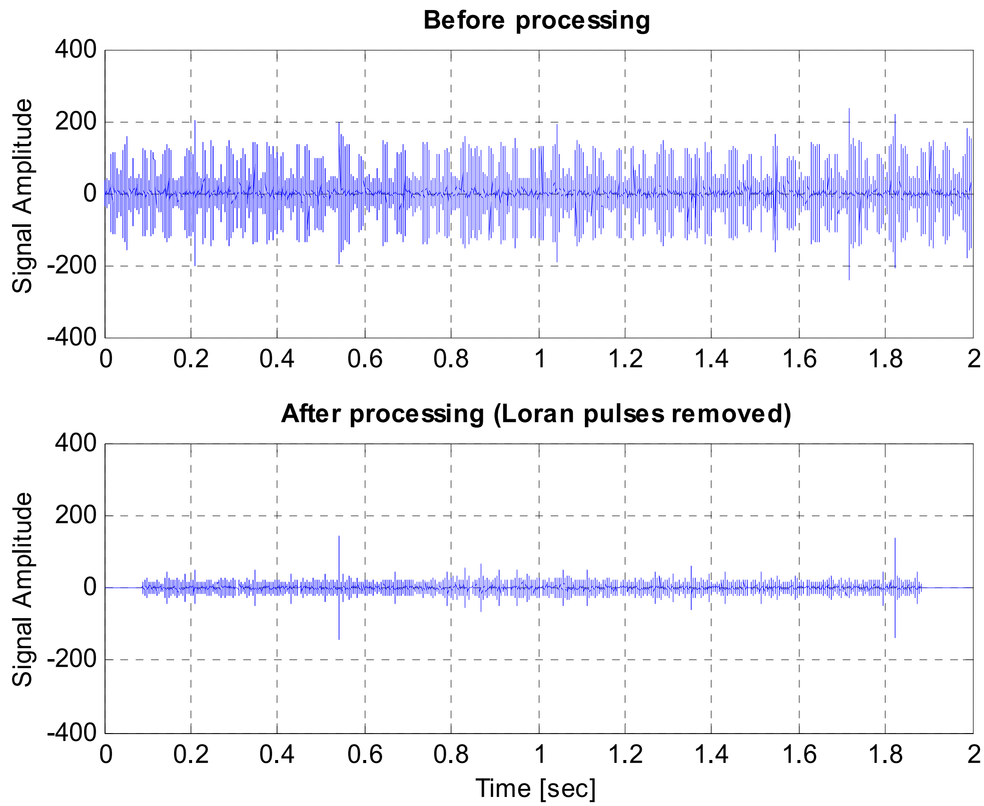

Figure 5.18 H-field antenna channel before (top-plot) and after (bottom plot) removal of Loran pulses for the first flight test

As mentioned earlier, the entire data set is processed in a similar way. The calculated RMS values of the Master, Z Secondary, and noise for every 2-second data block are plotted in Figure 5.19 for the entire 326-second data set. The noise floor is fairly stable throughout the data set. RMS value for the Z Secondary dropped to zero for an instance due to significant difference in the signal strengths (less than 93%) of the two Secondaries after integrating PCIs.

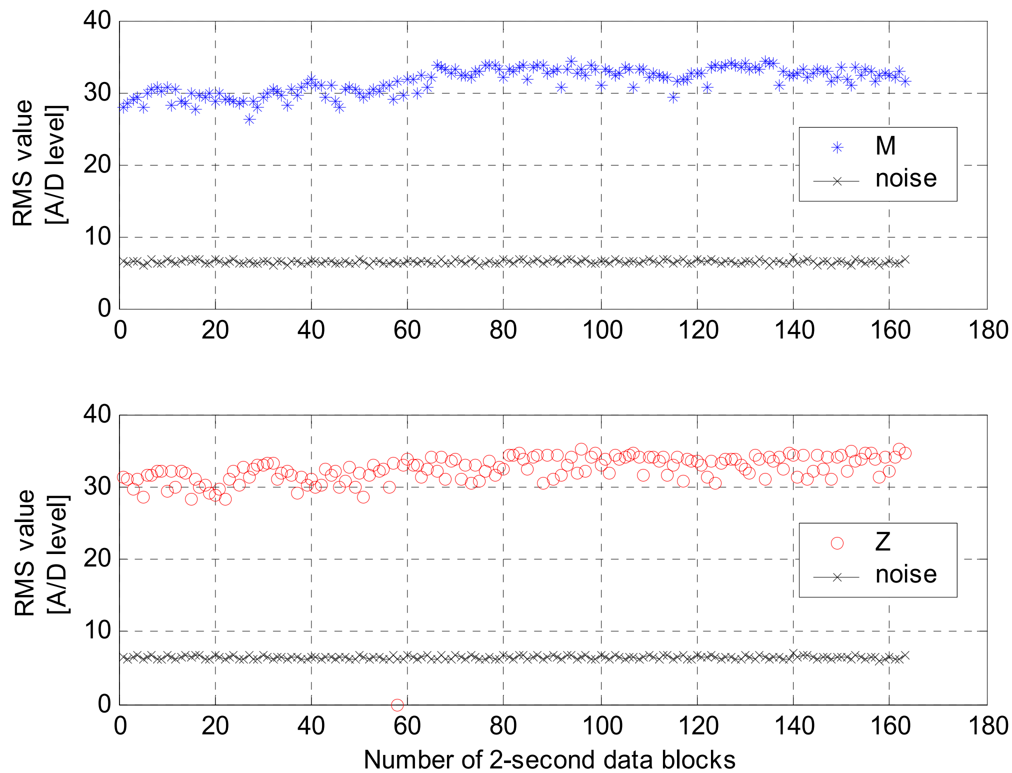

Figure 5.19 H-field antenna channel RMS values for Master, Z secondary (NEUS chain) and noise for the first flight test

Using the noise sequence, the noise distribution for the H-field is calculated and plotted in Figure 5.20. This distribution too like the E-field antenna channel noise distribution provides experimental data for probabilities as small as 10^{-7} (see Figure 5.21).

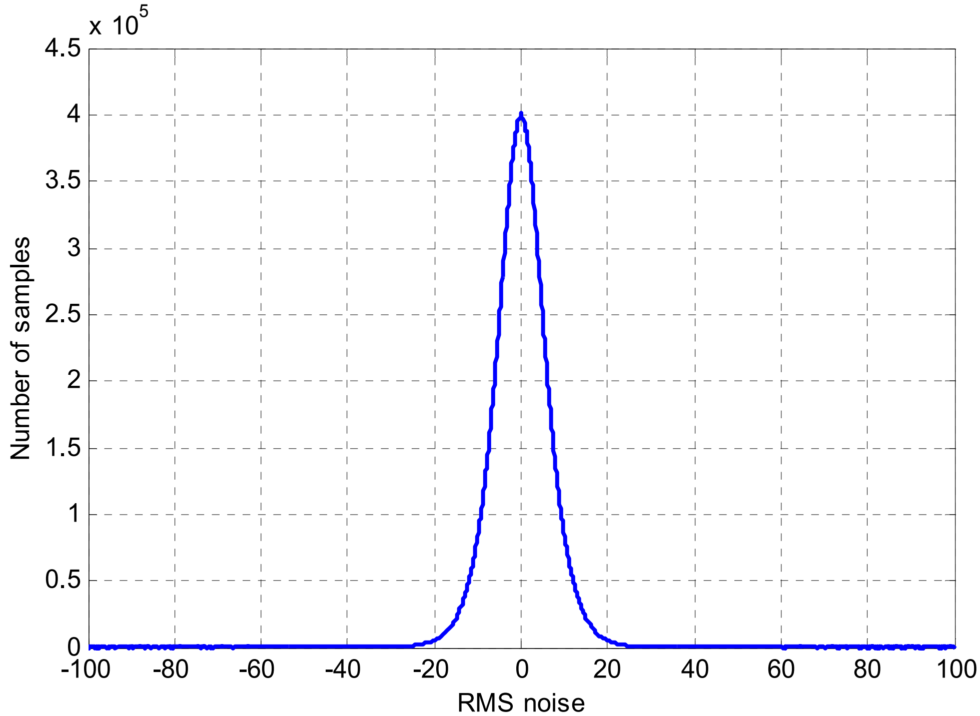

Figure 5.20 H-field antenna channel noise distribution for the first flight test

The cumulative distribution functions (cdf and 1.0 - cdf) of noise for the H-field antenna. are calculated and plotted against the Gaussian cdf (with the same standard deviation as the noise) in Figure 5.21. As discussed for the E-field noise statistics, the H-field statistics too indicate that the tail probabilities of the calculated noise cdf (and 1.0 - cdf) are larger than the Gaussian cdf (and 1.0 - cdf) with an equivalent rms value. Noise of the collected data can be overbounded by a Gaussian distribution that has 3.25 times the standard deviation of the collected noise.

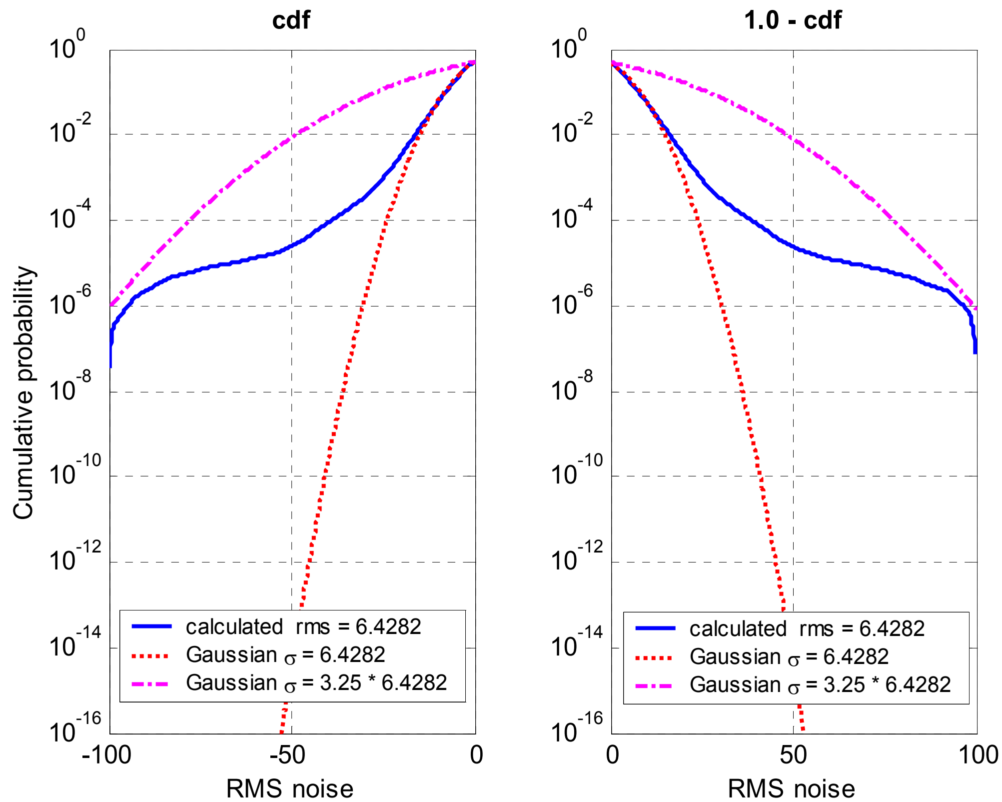

Figure 5.21 H-field antenna channel noise statistics for the first flight test

5.3 Comparison of the E-field and H-field Antenna Channel Data for the First Flight Test

The noise distribution and the noise statistics for the E-field and the H-field data closely match. Averaged SNR values (at the output of the antenna pre-amplifier) calculated after processing the collected data are provided in Table 5.1.

Table 5.1 Averaged SNR measurements for the first flight test

Antenna	SNR [dB] M (NEUS)	SNR [dB] Z (NEUS)
E-field	12.1	13.9
H-field	13.8	14

From Table 5.1, it follows that the calculated SNR values for the E-field and the H-field antenna are almost equal.

6 FLIGHT TEST II (THUNDERSTORM CONDITIONS)

The second flight test was conducted under thunderstorm conditions near Orlando, Florida on August 14, 2003 from 12:29:32 to 12:34:56 local time. The airborne data were collected at an ellipsoidal (WGS-84) height of approximately 5 km in the vicinity of thunderstorms. Figure 6.1 (left) shows the flight trajectory obtained from GPS while the right image shows a radar snapshot of the thunderstorm activity that occurred during the period in which the above data were collected.

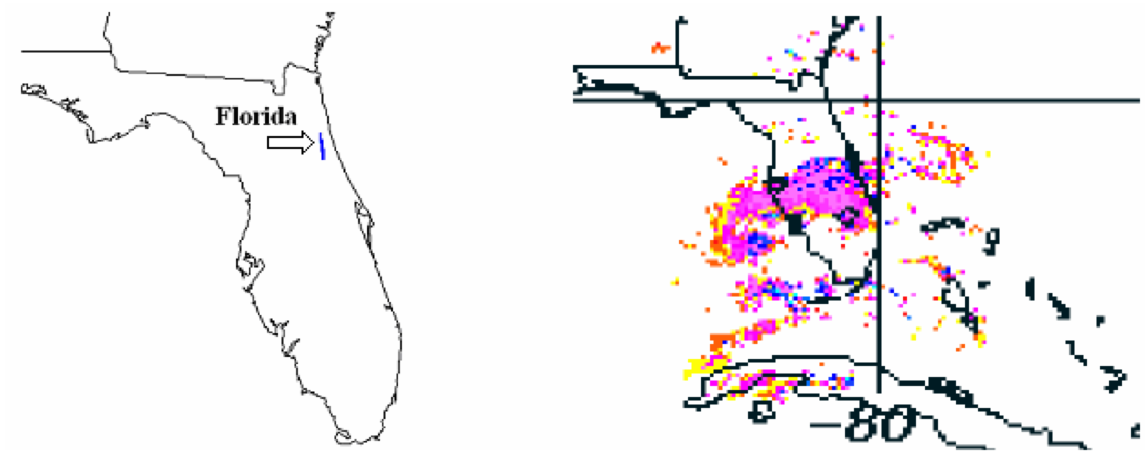

Figure 6.1 Flight test trajectory and Radar image of thunderstorm activity near Orlando International Airport

South-East U.S. (SEUS) chain transmitter locations are shown in Figure 6.2. At several instances the data was affected by lightning discharges from the thunderstorm. A Multiplication factor of 6.1 is used for removal of thunderstorm bursts (as explained in section 4.2) for the E-field and the H-field data. This factor was set after considering the noise floor of the data and was found to be an effective value for removing thunderstorm bursts. The results are discussed in the next section.

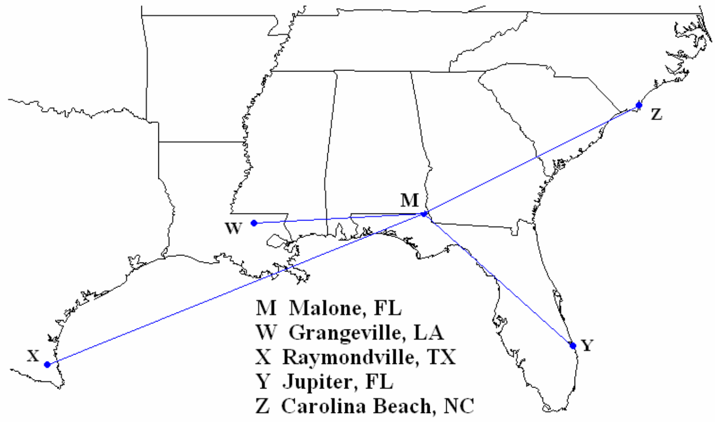

Figure 6.2 South-East U.S. Loran-C chain

6.1 E-field Antenna Channel Results for Second Flight Test

The data were collected in close proximity of thunderstorms and Figure 6.3 shows an example of the E-field data that were affected by lightning strikes. The effects of the lightning strikes can be clearly seen as spikes in the time domain signal.

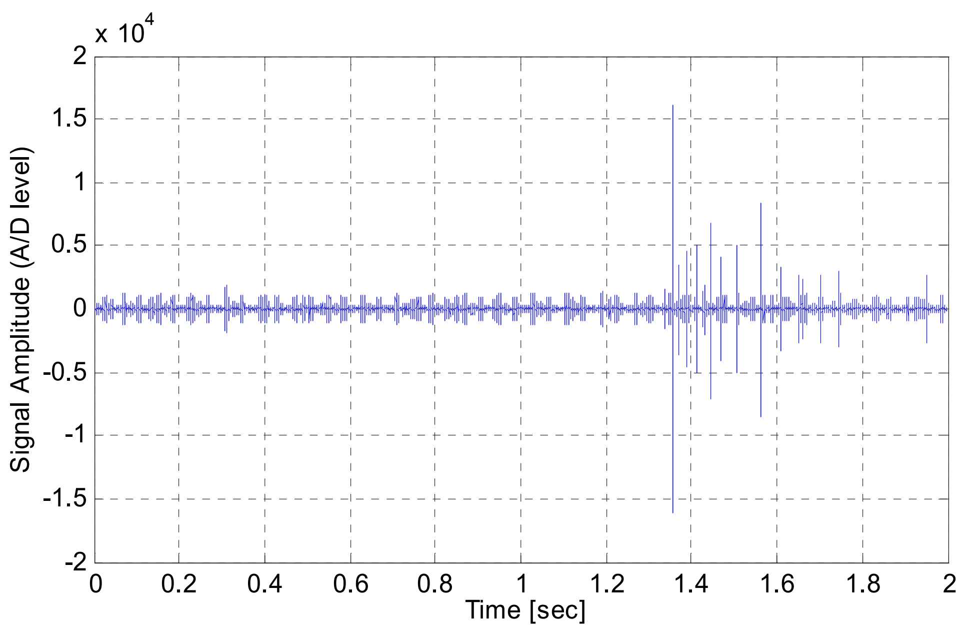

Figure 6.3 E-field antenna data example with short duration, large amplitude lightning noise for the second flight test

Figure 6.4 shows a zoomed-in version of Figure 6.3. A Secondary station pulse affected by the lightning strike can be observed in Figure 6.4.

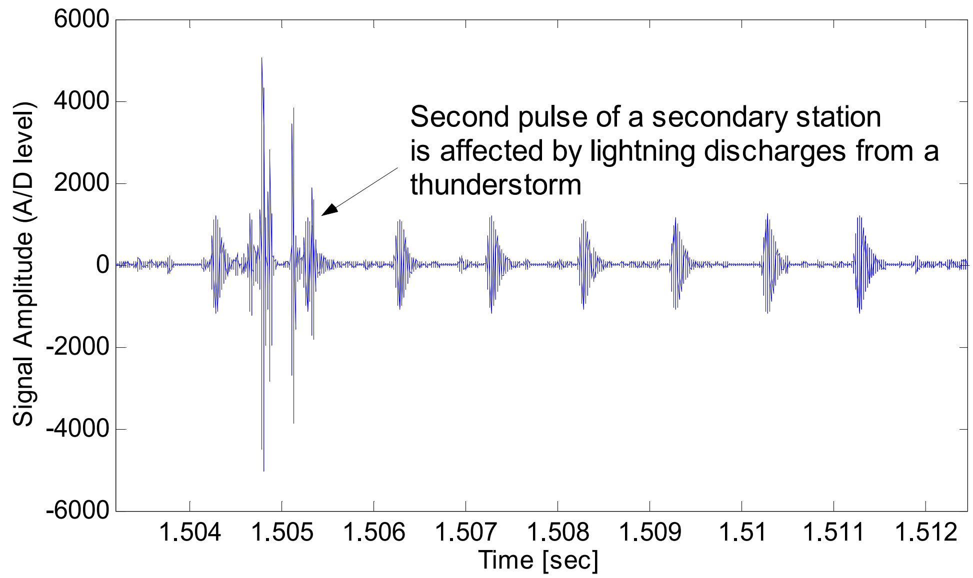

Figure 6.4 E-field antenna data example focusing on the affected pulse of secondary due to thunderstorm for the second flight test

Figure 6.5 depicts a scenario where the thunderstorm had a sustained energy over a larger time interval. Unlike Figure 6.4 where a pulse of a Secondary station was affected, this one did not affect any Loran pulse.

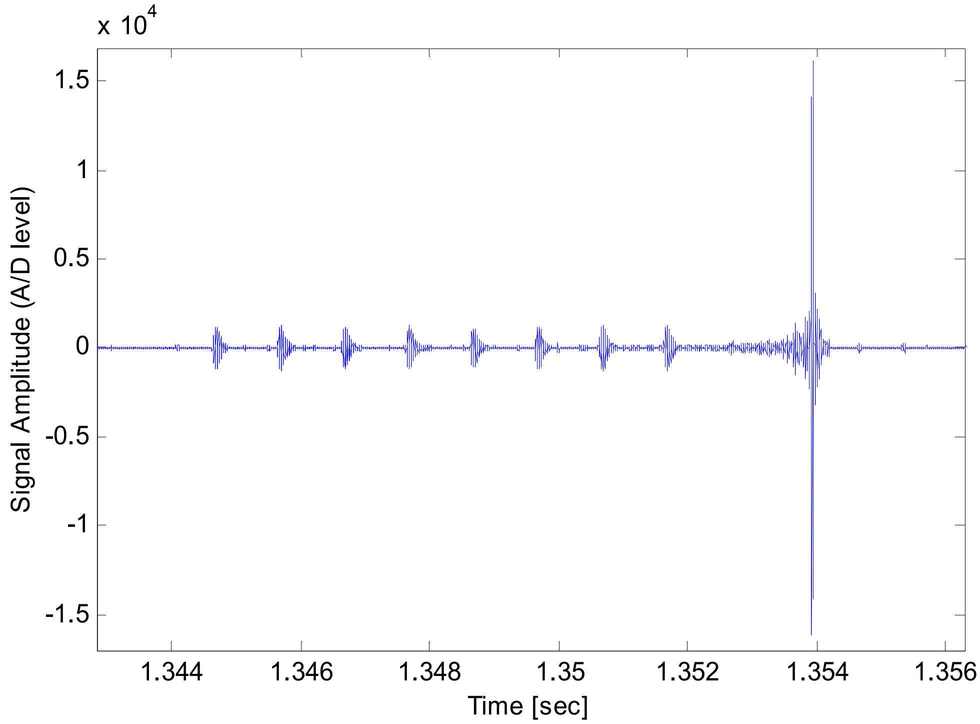

Figure 6.5 E-field antenna data example focusing on relatively large-duration, large amplitude lightning noise for the second flight test

The data are processed in a similar way as discussed in Chapter 4. The 2-second data block shown in Figure 6.3 is affected by mild thunderstorm activity and it can be processed for the SNR calculation and the noise characterization. Figure 6.6 shows the 2-second signal envelope after removal of NB and CW interferences. The effect of bin removal using energy estimation (as discussed in Chapter 4) can be seen in the latter half of the 2-second data block shown in Figure 6.6.

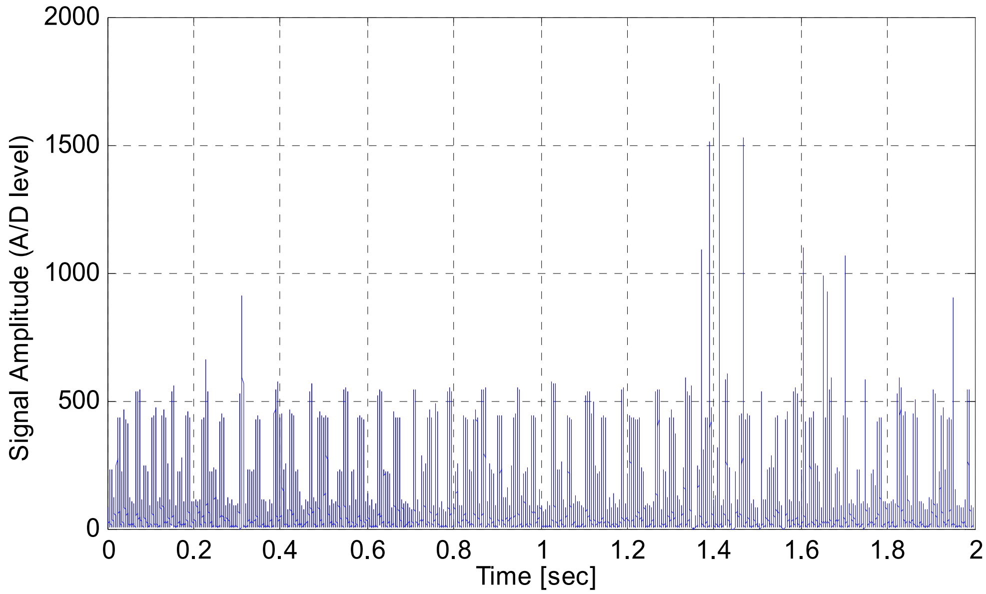

Figure 6.6 E-field antenna channel signal envelope for the second flight test

The next step of the processing involves integrating PCIs for different chains. Figure 6.7 shows the signal obtained after integrating the PCIs for the SEUS chain. The data were collected near Palm Coast, Florida and so the SEUS chain provided better coverage than any other chain. The Master (located in Malone, FL) and the Y Secondary (located in Jupiter, FL) were the closest transmitters and so the SNR values were computed for them. Figure 6.7 shows the plot obtained after integrating the PCIs for the SEUS chain. Two occurrences of the Master, Y Secondary and the Z Secondary can be seen in Figure 6.7.

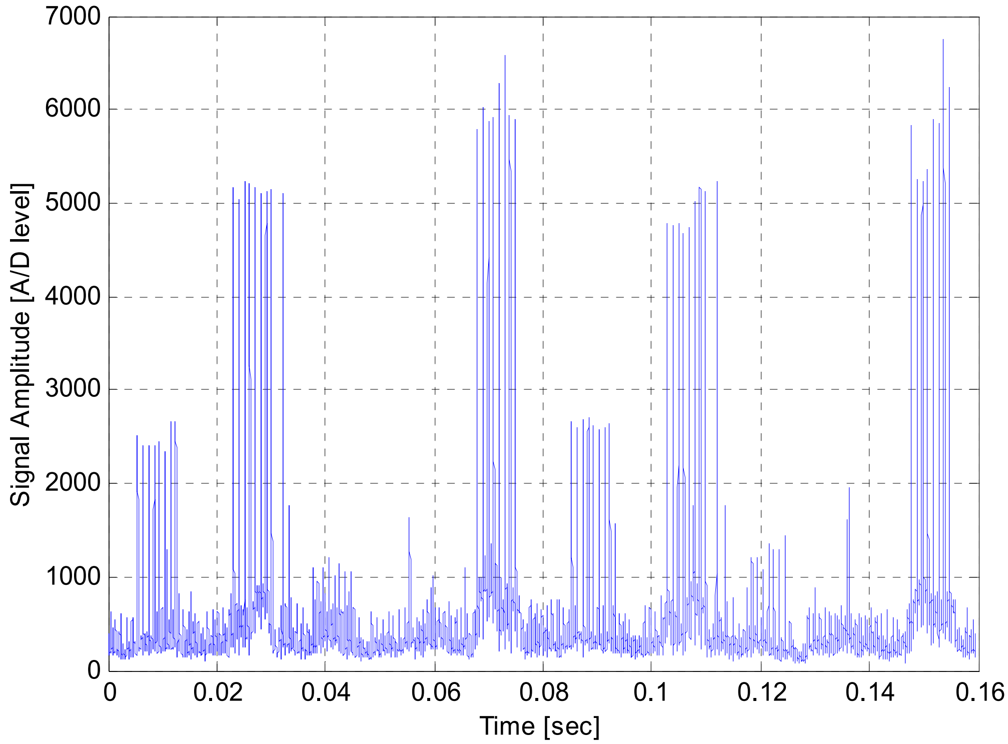

Figure 6.7 E-field antenna channel data after integrating the PCIs for the SEUS chain for the second flight test

Similarly, the PCIs for other chains are integrated for station identification. The identified Loran chains are then removed to calculate the noise sequence and characterize the noise. The top plot of Figure 6.8 shows the received signal before removal of the Loran pulses, while the bottom plot shows the noise sequence after removal of the Loran pulses.

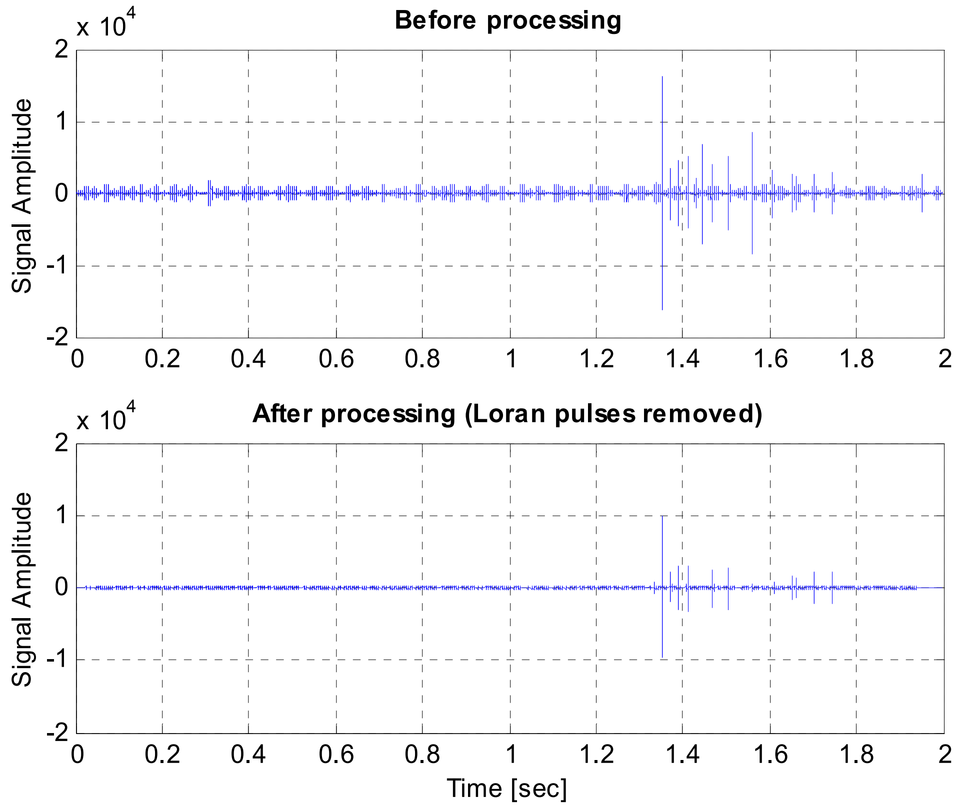

Figure 6.8 E-field antenna channel before (top plot) and after (bottom plot) removal of Loran pulses for the second flight test

The entire data set is processed in a similar way and the calculated RMS values of the Master, Y Secondary, and noise for every 2-second data block are plotted. Figure 6.9 shows such a plot for the entire 326-second (2×163) data set. The RMS value for the master dropped to zero for one instance due to a significant difference in the signal strengths (less than 93%) of the two Masters after integrating PCIs. Note the increase in RMS value of the Master and the decrease in RMS value in the Y Secondary. It is due to the increase in signal strength of the Master station as the distance between the aircraft and the Master transmitter decreased. The reverse is valid for the Y Secondary.

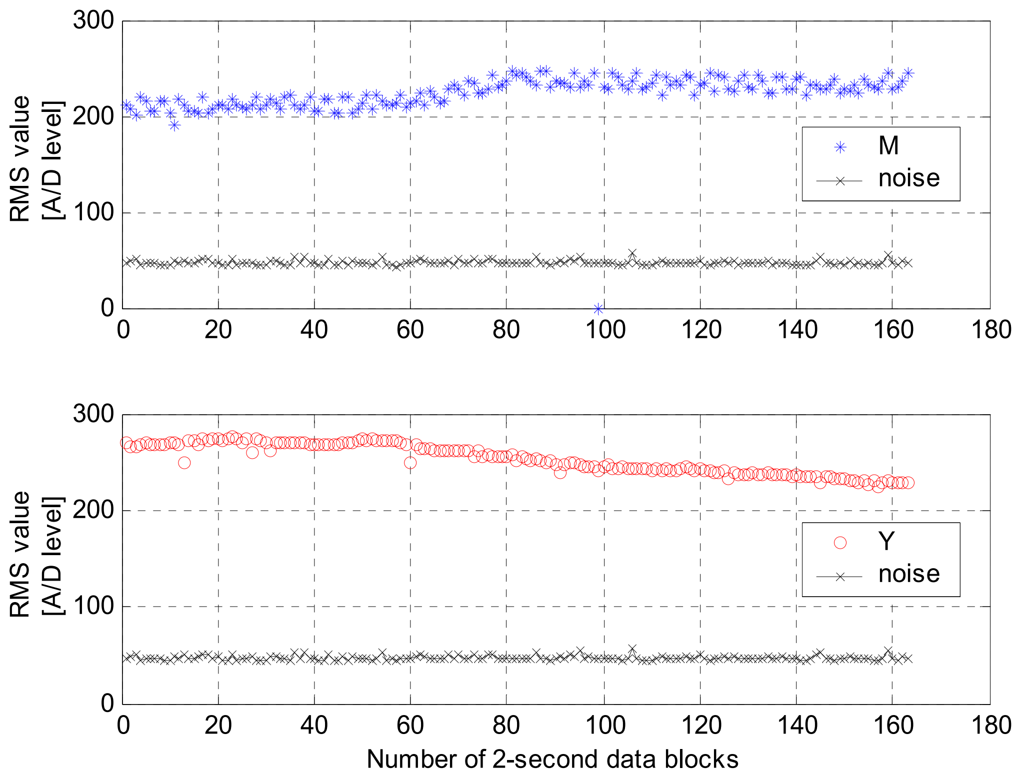

Figure 6.9 E-field antenna channel RMS values for Master, Y secondary (SEUS chain) and noise for the second flight test

Next, the distribution of the noise samples for the entire 326-second data set is computed (see Figure 6.10). Note that the σ value for noise of 60 was chosen for this case since the noise floor was higher compared to the first flight test. The peak in the center of the distribution is due to large number of samples that have a value close to zero.

From the noise distribution, the cdf and (1.0 - cdf) are calculated and plotted against the Gaussian cdf (with the same standard deviation as the noise) in Figure 6.11. The plot indicates that the tail probabilities of the calculated cdf and (1.0 - cdf) are larger than the Gaussian cdf and (1.0 - cdf) with an equivalent rms value. Similar to the results of the first flight test, the collected noise can be overbounded by a Gaussian distribution that has three times the standard deviation of the collected noise.

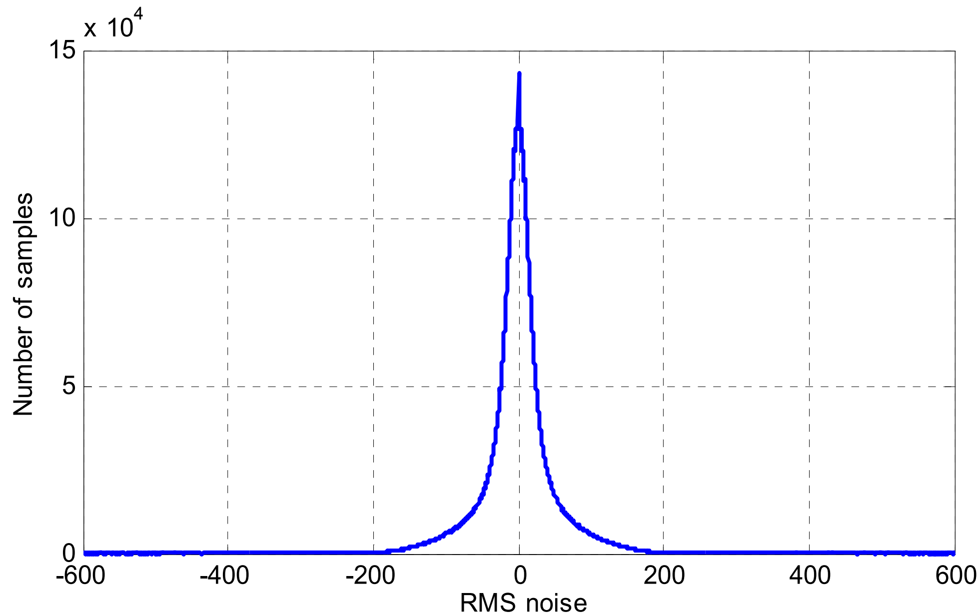

Figure 6.10 E-field antenna channel noise distribution for the second flight test

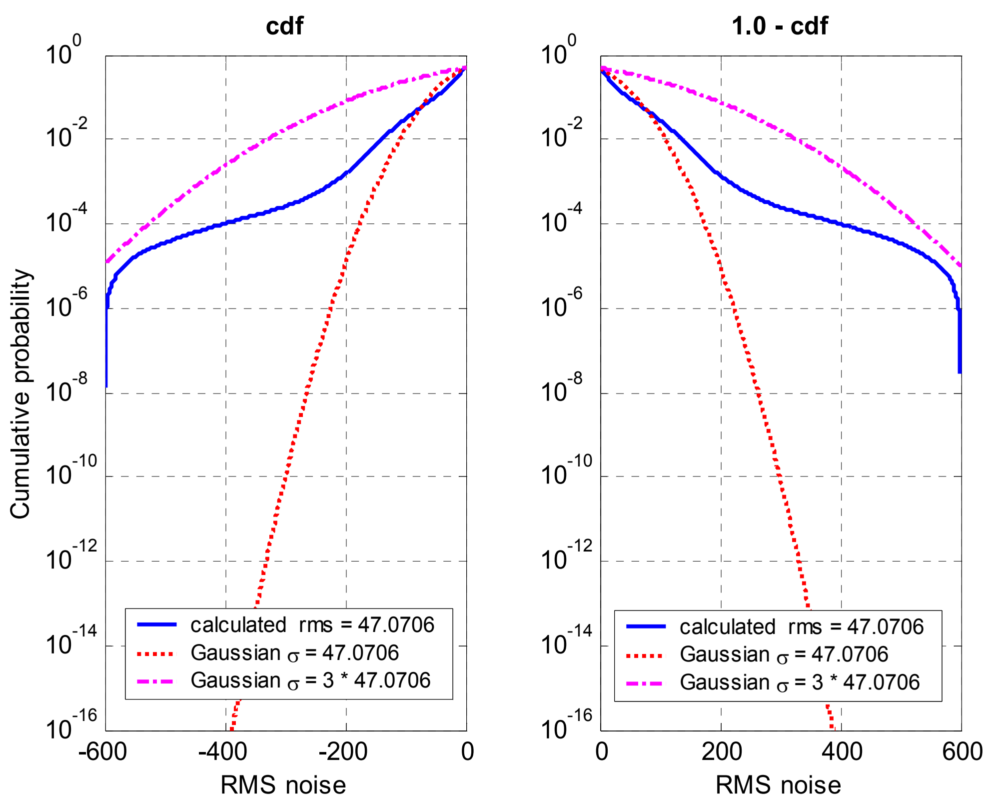

Figure 6.11 E-field antenna channel noise statistics for the second flight test

6.2 H-field Antenna Channel Results for Second Flight Test

The data were collected in vicinity of thunderstorms and as expected, the effects of the lightning strikes for the H-field antenna are similar to the E-field antenna. The effects of the lightning strikes can be clearly seen as spikes in the time domain signal. Figure 6.12 shows an example of a 2-second H-field data block that was affected by lightning strikes.

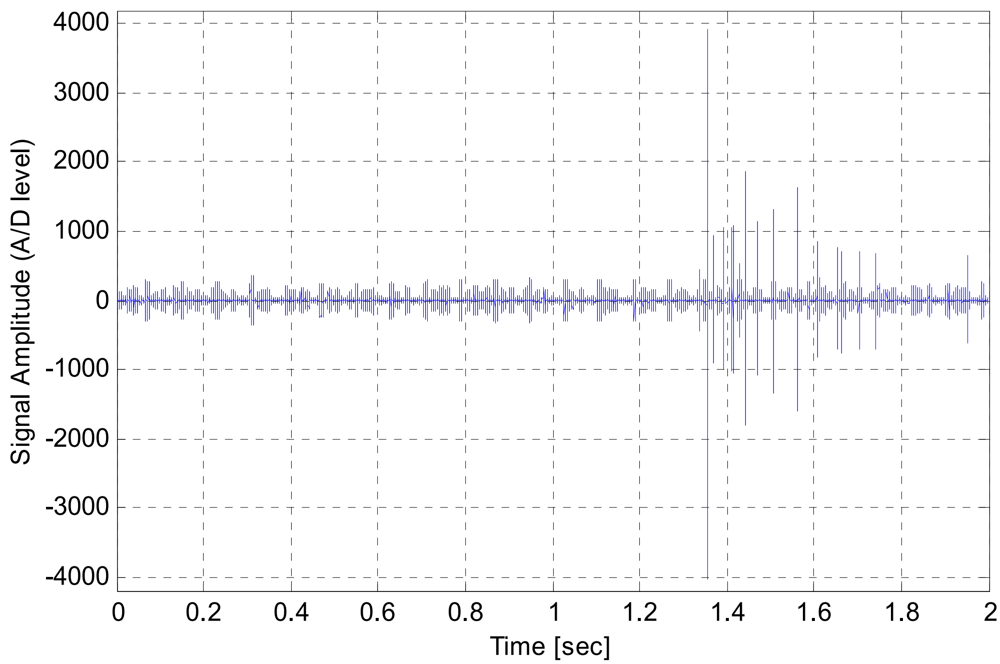

Figure 6.12 H-field antenna data example with short duration, large amplitude lightning noise for the second flight test

Figure 6.13 shows the zoomed-in version of Figure 6.12. A Secondary station pulse affected by the lightning strike can be observed in Figure 6.13.

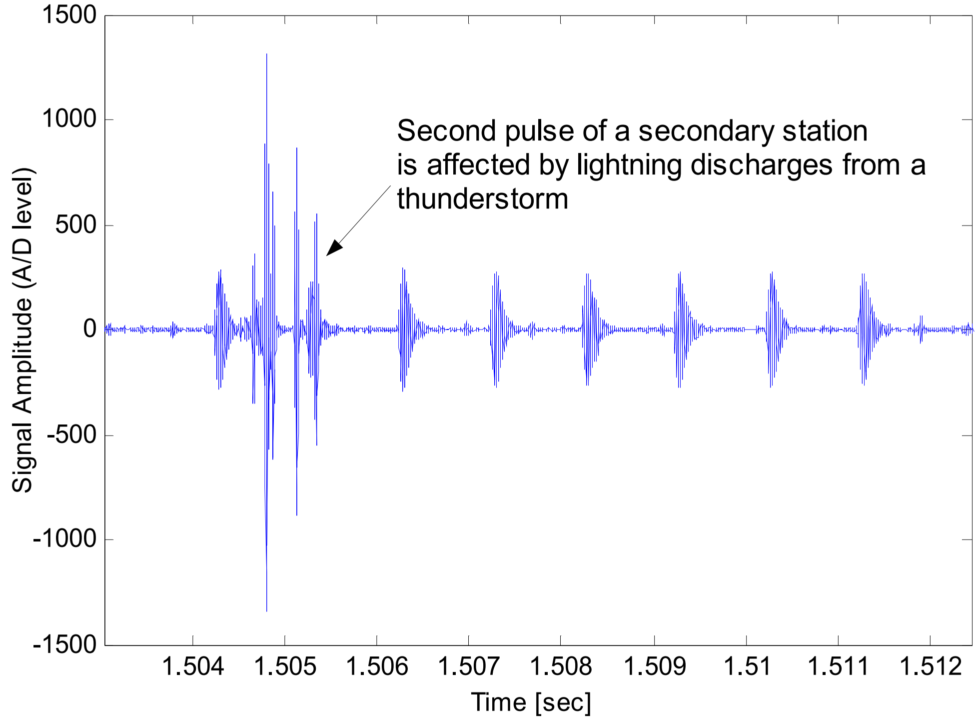

Figure 6.13 H-field antenna data example focusing on the affected pulse of secondary due to thunderstorm for the second flight test

Figure 6.14 depicts a case where the thunderstorm had a sustained energy over a larger interval. The noise floor in this case is increased; however, unlike Figure 6.13, the lightning does not have any impact on the secondary pulses. The results are identical to those of the E-field antenna.

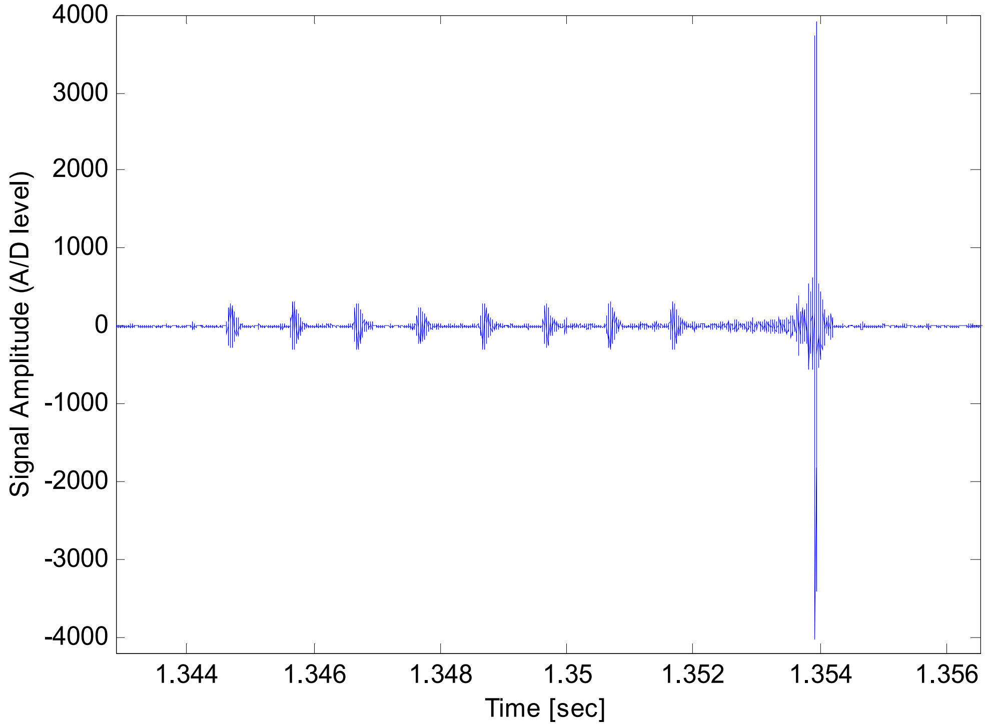

Figure 6.14 H-field antenna data example focusing on relatively large-duration, large amplitude lightning noise for the second flight test

Next, the data is processed in a similar way as discussed in Section 6.1. The 2-second data block shown in Figure 6.12 is affected by mild thunderstorm activity and can be processed just as the E-field in the previous section was processed. Figure 6.15 shows the 2-second signal envelope after removal of NB and CW interferences. Similar to the E-field data, the effect of bin removal using energy estimation can be seen in the latter half of the 2-second data block shown in Figure 6.15.

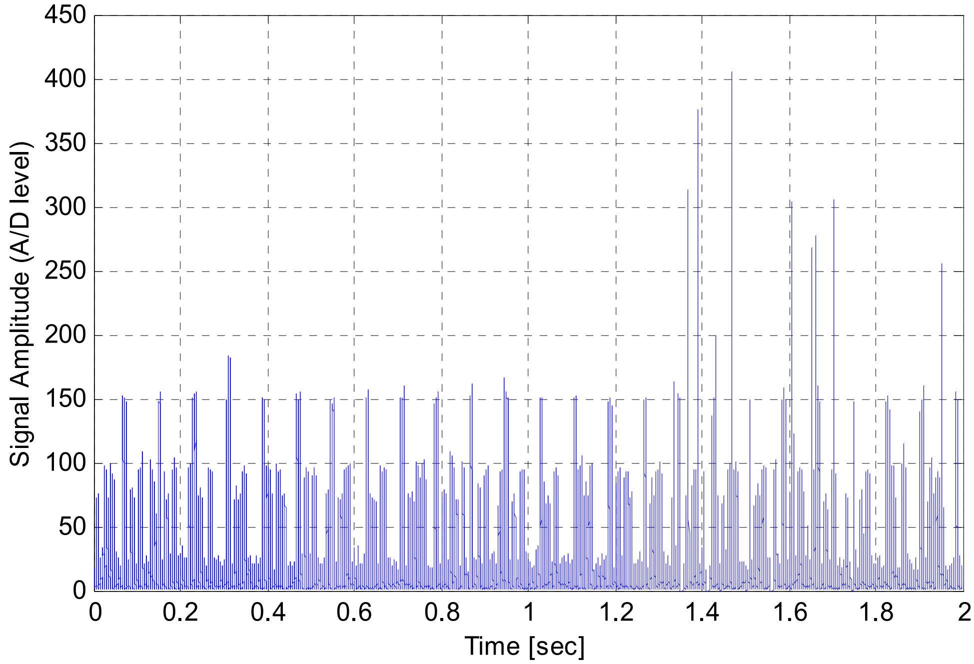

Figure 6.15 H-field antenna channel signal envelope for the second flight test

The next step of the processing involves integrating PCIs for different chains. Figure 6.16 shows the signal obtained after integrating the PCIs for the SEUS chain. The results are identical to the E-field data discussed in the previous section.

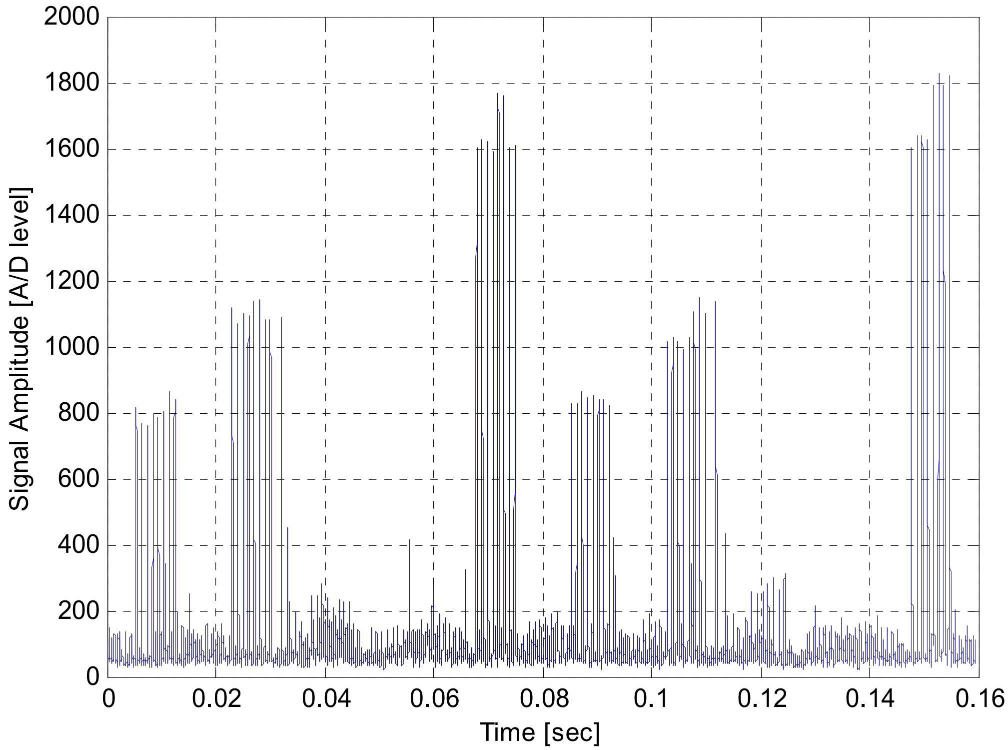

Figure 6.16 H-field antenna channel data after integrating the PCIs for the SEUS chain for the second flight test

In a similar way, the PCIs for other chains are integrated for pulse identification. The identified Loran chains are then removed to calculate the noise sequence and characterize the noise. The top plot of Figure 6.17 shows the received signal before removal of the Loran pulses, while the bottom plot shows the noise sequence after removal of the Loran pulses.

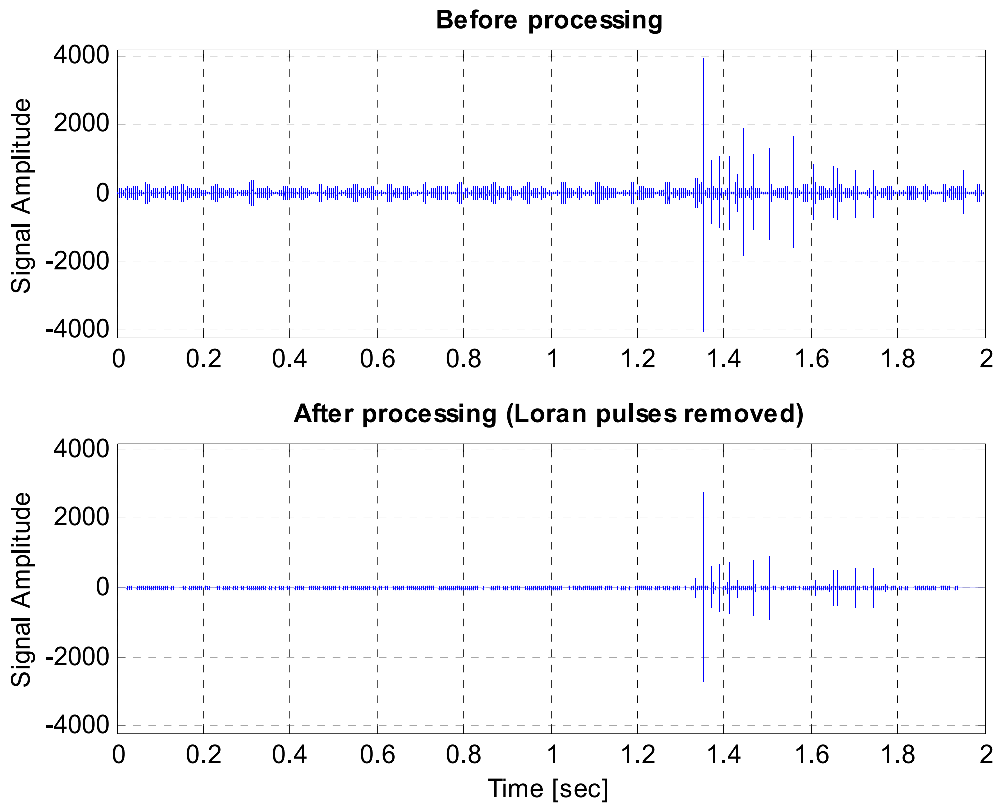

Figure 6.17 H-field antenna channel before (top plot) and after (bottom plot) removal of Loran pulses for the second flight test

After the entire data set is processed, the calculated RMS values of the Master, Y Secondary, and noise for every 2-second data block are plotted. Figure 6.18 shows such a plot for the entire 326-second data set. Note the increase in RMS value of the Master and the decrease in RMS value in the Y Secondary. This is identical to the trend obtained for the E-field data. It is due to the increase in signal strength of the Master station as the distance between the aircraft and the Master transmitter decreased. The reverse is valid for the Y Secondary.

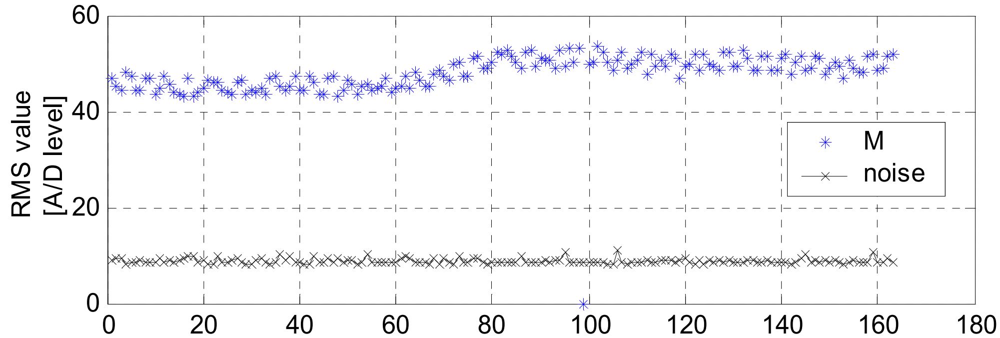

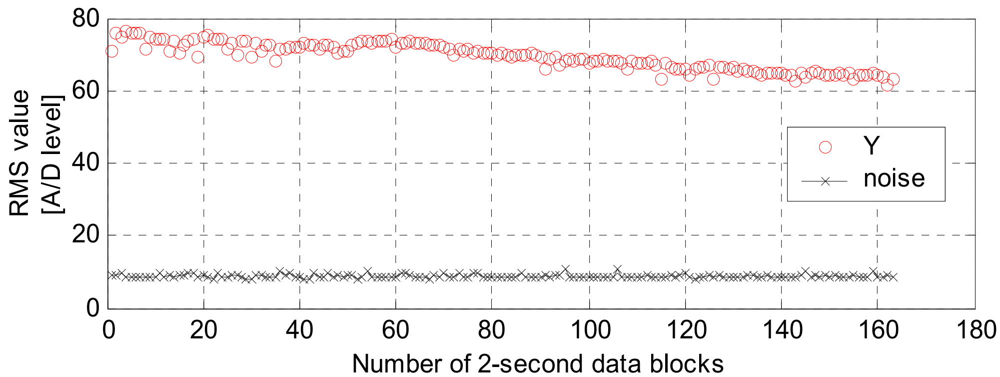

Figure 6.18 E-field antenna channel RMS values for Master, Y secondary (SEUS chain) and noise for the second flight test

Next, the distribution of the noise samples for the entire data set is computed as shown in Figure 6.19. Similar to the E-field noise distribution, the peak in the center of the distribution is due to large number of samples that have a value close to zero.

From the noise distribution, the cdf and (1.0 - cdf) are calculated and plotted against the Gaussian cdf (with the same standard deviation as the noise) in Figure 6.20. The plot indicates that the tail probabilities of the calculated cdf and (1.0 - cdf) are larger than the Gaussian cdf and (1.0 - cdf) with an equivalent rms value. As mentioned earlier, the collected noise can be overbounded by a Gaussian distribution that has three times the standard deviation of the collected noise.

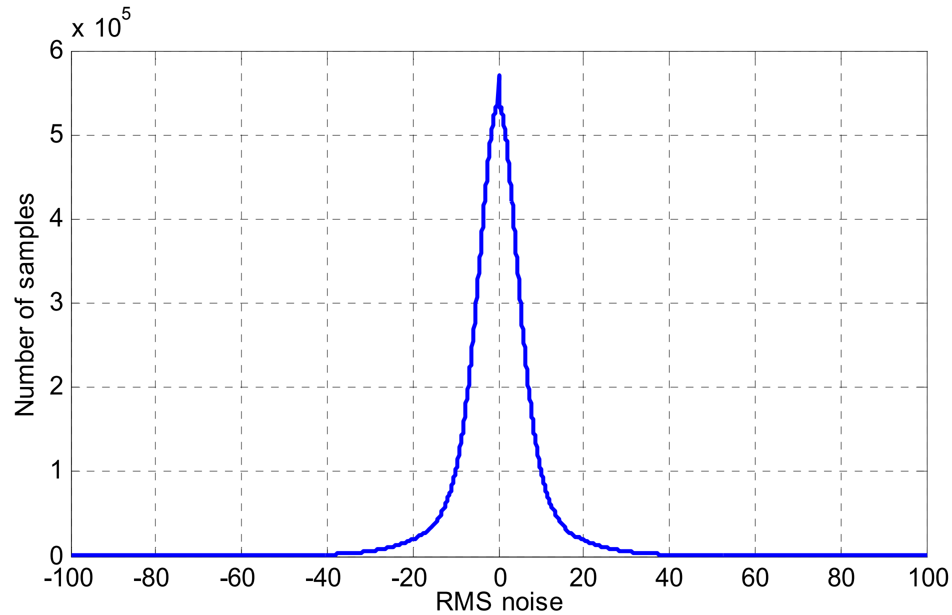

Figure 6.19 H-field antenna channel noise distribution for the second flight test

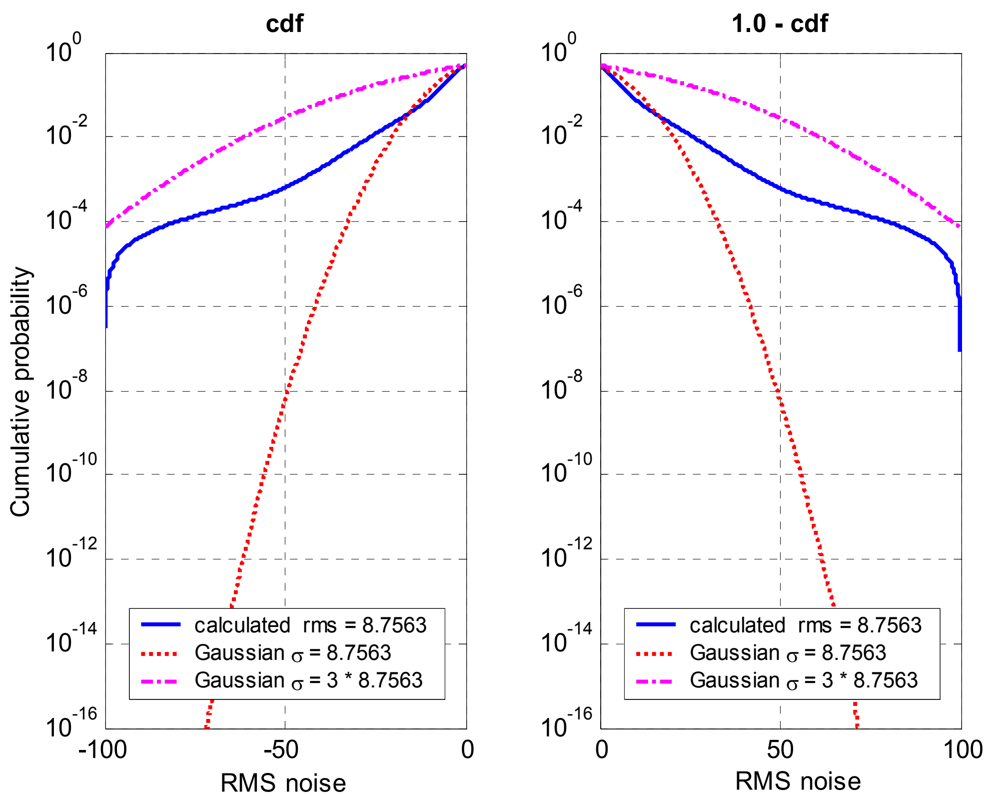

Figure 6.20 H-field antenna channel noise statistics for the second flight test

6.3 Comparison of the E-field and H-field Antenna Channel Data for Second Flight Test

From sections 6.1 and 6.2, the noise distribution and the noise statistics for the E-field and the H-field data closely match. Averaged SNR values (at the output of the antenna pre-amplifier) calculated after processing the collected data are provided in Table 6.1.

Table 6.1 Averaged SNR measurements for the second flight test

Antenna	SNR [dB] M (SEUS)	SNR [dB] Y (SEUS)
E-field	13.6	14.6
H-field	14.8	18

Gain advantage of the H-field antenna over the E-field antenna can be noticed from the SNR values of the Master and the Secondary station.

6.4 Comparison of Noise for First and Second Flight Tests

Based on the results obtained from the first and second flight tests, it can be observed that Loran can still be used in the presence of thunderstorm activity, with only a small increase in the received noise power. In the presence of thunderstorms, noise increase for both antennas was less than 2.3 dB. The cumulative distribution functions for both E-field and H-field antennas, for both flight tests, closely match in shape.

Analysis of additional data sets affected by thunderstorm conditions along with the data obtained from the StormScope and the National Lightning Detection Network (NLDN) would provide an increased understanding of the lightning influence on Loran for aviation applications. Moreover, simultaneous data collection in flight and on the ground would provide results on the impact of thunderstorms on Loran in flight compared to Loran performance for terrestrial receivers [22].

7 FLIGHT TEST III (PRECIPITATION STATIC CONDITIONS)

Precipitation static (P-Static) caused by charging of aircraft during flight through rain, snow, ice, dust, or sand can lead to radio noise generated by the electrical discharge from the aircraft, or between aircraft components. This high-voltage, low-current discharge can cause severe degradation of the Loran signal quality if an E-field antenna is used. Various publications [2, 13-16, 21] have reported the effects of and mitigation of P-Static using an H-field antenna.

This chapter details the comparative performance of the E-field and the H-field antenna during a severe P-Static flight condition. The airborne data were collected in Michigan on January 21, 2004 from 13:35:54 to 13:41:18 local time. Figure 7.1 shows the flight trajectory in Michigan. The airborne data were collected at an ellipsoidal (WGS-84) height of approximately 1.5 km. The temperature was near the freezing point, the humidity was low, and the aircraft was maneuvered to maximize exposure to a snow cloud.

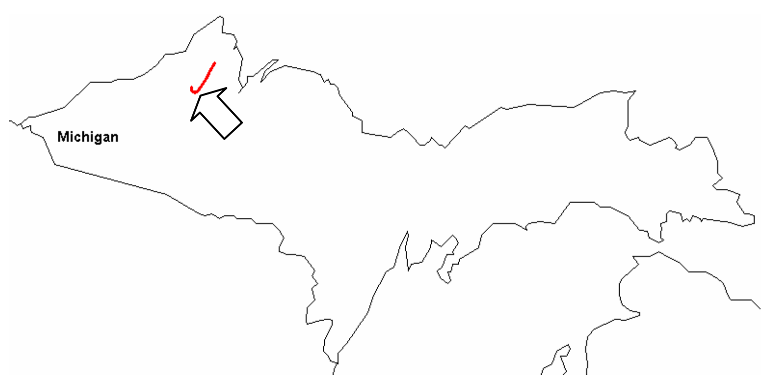

Figure 7.1 Flight trajectory for the third flight test

The data processing software developed for characterizing noise that was used for the first two data sets is not used for this data set due to very high noise level. Instead, the data are normalized to the maximum A/D converter levels to analyze the effect of noise. In other words, the amplitude of the sampled data is scaled to ± 1.0. To compare the effect of P-Static with the normal (no P-Static) conditions, power for each 2-second data block is calculated and normalized to normal (no P-Static) conditions.

7.1 Third Flight Test Data Example: No P-Static

The airborne data indicate severe P-Static during the middle half of the data set. For the first two minutes, the data set had no P-Static effects. Figure 7.2 shows one such instance where the P-Static did not influence the 2-second data record. Two normal Loran pulses can clearly be seen in the Figure. As mentioned previously, the amplitude is the normalized signal amplitude. The calculated normalized power is displayed on the top of each plot.

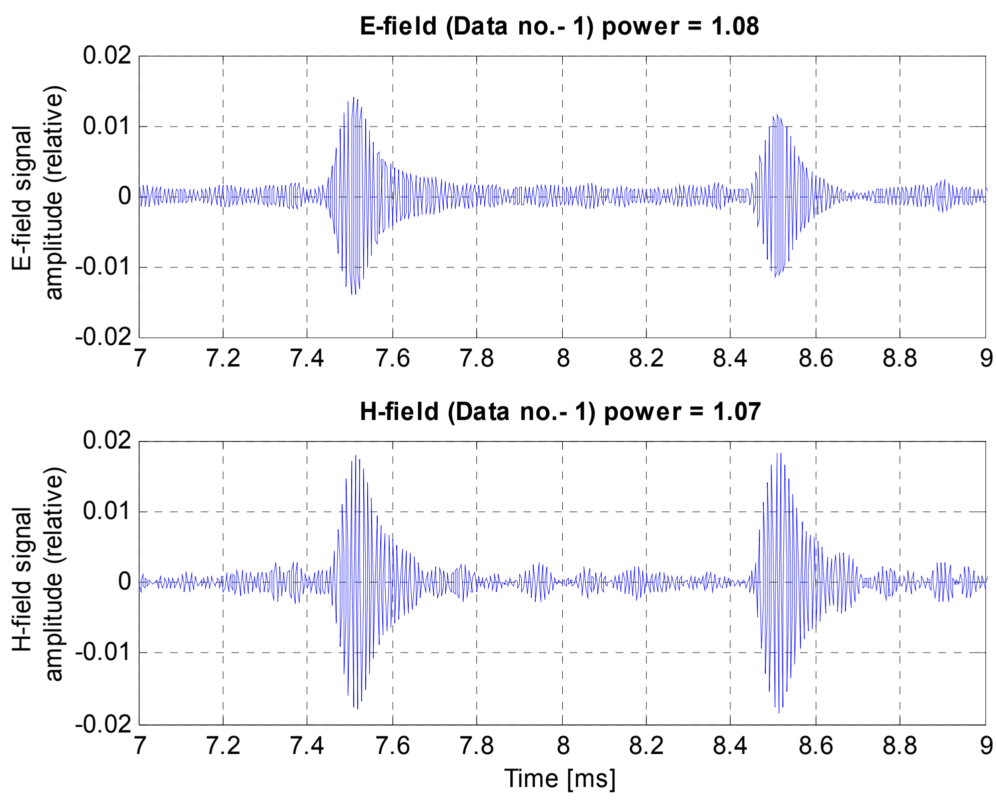

Figure 7.2 E-field and H-field data during no P-Static conditions for the third flight-test

7.2 Third Flight Test Data Example: Light P-Static

This section describes the performance of E-field and the H-field antennas in light P-Static conditions. Figure 7.3 shows one such instance of light P-static conditions. A noticeable effect can be seen on the E-field signal. The noise power has increased by a factor of five. Thus, the SNR for this case would be degraded.

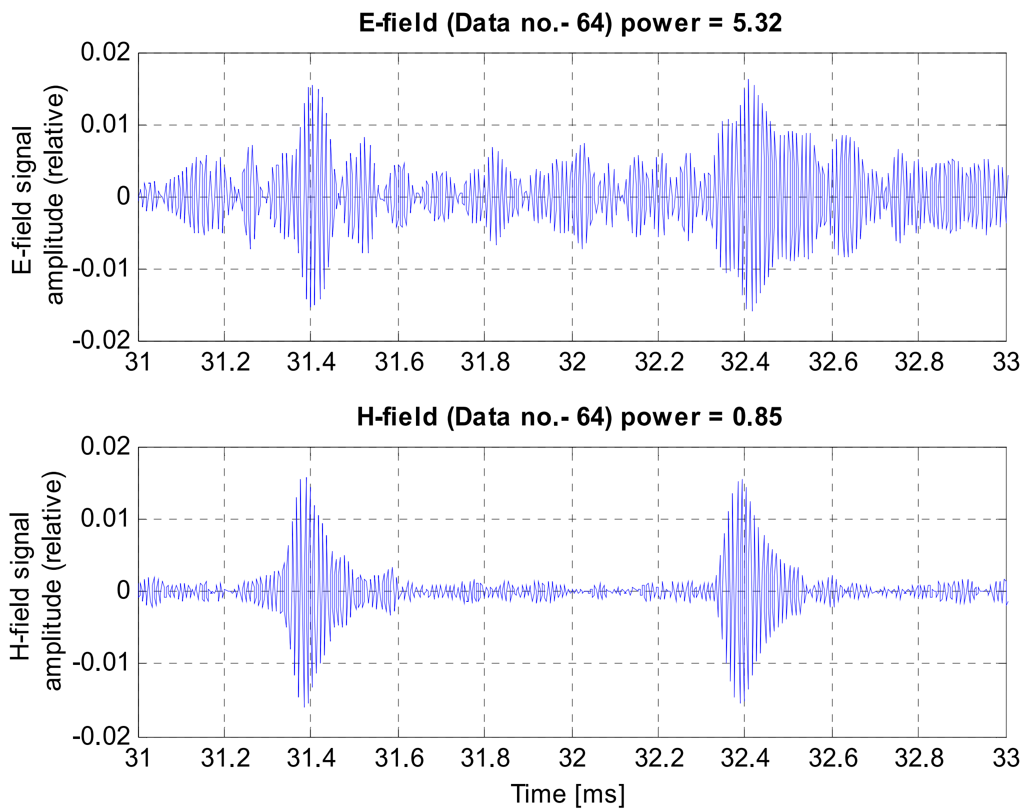

Figure 7.3 E-field and H-field data during light P-Static conditions for the third flight-test

However, there is no influence of the light P-Static condition on the H-field signal.

7.3 Third Flight Test Data Example: Moderate P-Static

Figure 7.4 shows the E-field and H-field antenna performance in moderate P-static conditions. The noise power on the E-field has increased by a factor of 13 compared to normal (no P-Static) conditions. The SNR in this case would be further degraded.

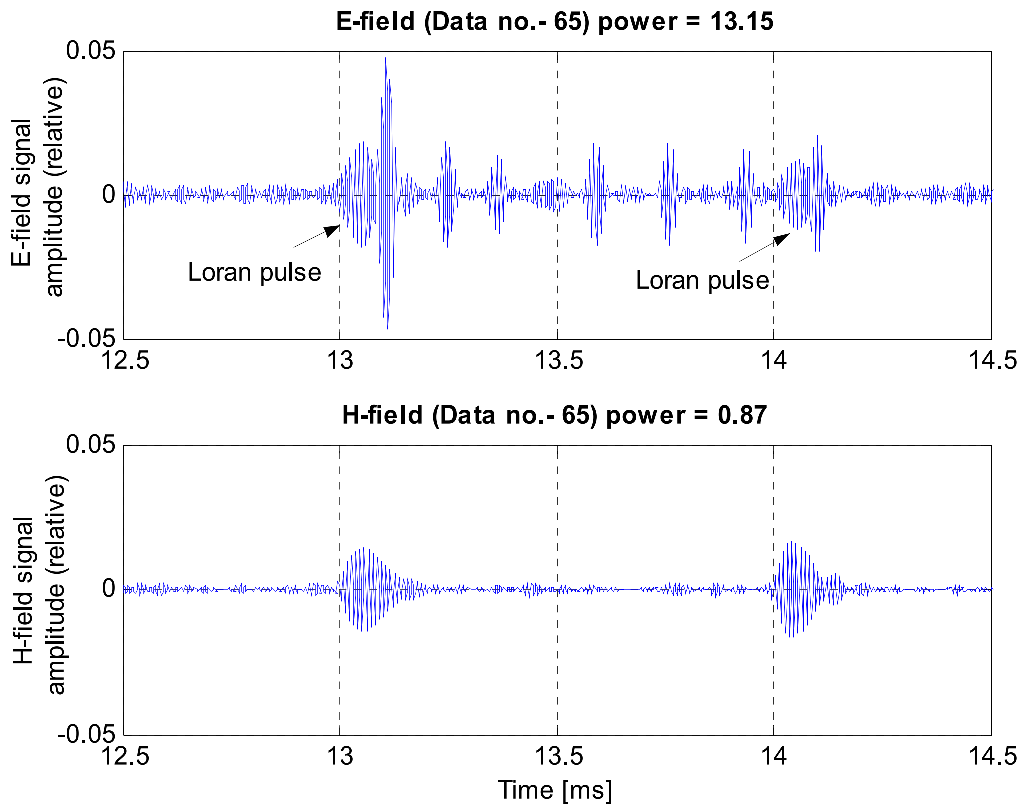

Figure 7.4 E-field and H-field data during moderate P-Static conditions for the third flight-test

In this case too, the moderate P-Static condition had no effect on the H-field signal.

7.4 Flight Test Data Example: Severe P-Static

This section describes the worst case scenario observed to date during P-Static. Figure 7.5 shows an instance where the E-field and H-field were influenced by severe P-static. As seen in the top plot of Figure 7.5, the E-field antenna channel A/D converter is close to saturation, the noise power has increased by a factor of about 136,629 (51 dB). In other words, the noise power for the E-field has increased by up to 51 dB with respect to normal conditions. Unlike the previous cases, the E-field data cannot be used as it is severely affected by broadband noise.

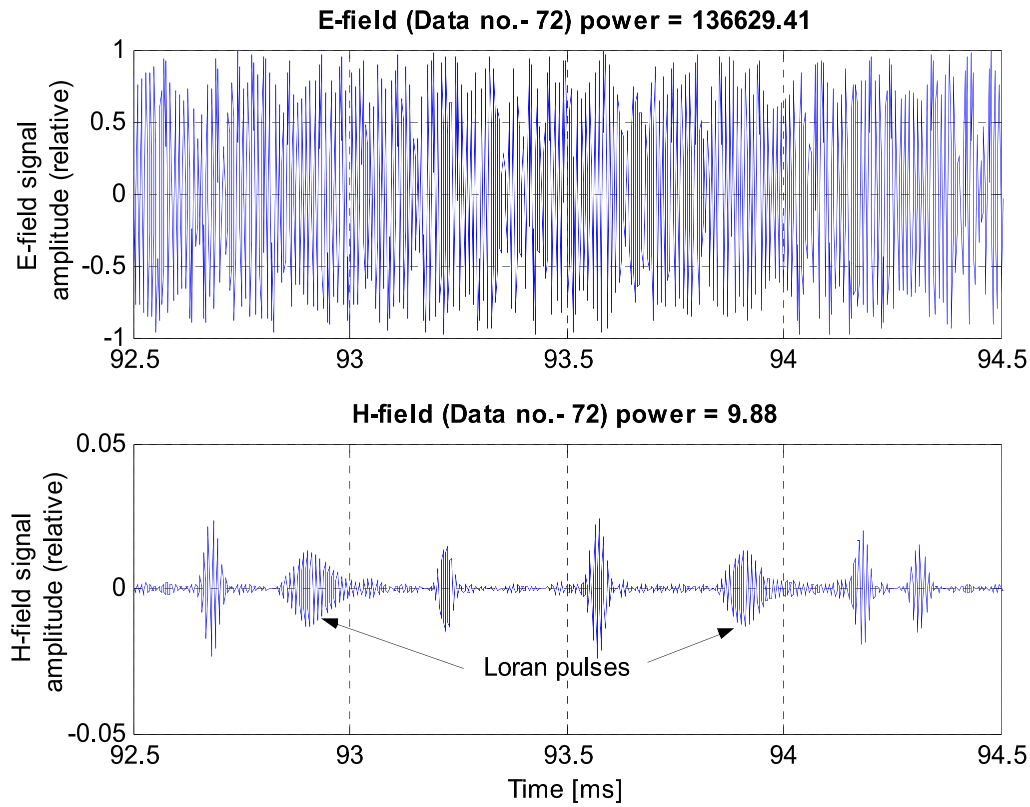

Figure 7.5 E-field and H-field data during severe P-Static conditions for the third flight-test

H-field for this case is also affected by the P-static; however, the H-field signal can still be used. Noise power has increased by a factor of 10, but the noise is pulsed at approximately 1 kHz thus affecting less than 1-out-of-5 pulses (on average). This results in an effective SNR degradation of less than 1 dB.

7.5 Power Profiles and Discharge Rate for the Third Flight Test

The entire 326-second flight data were processed and the power profile thus obtained is shown in Figure 7.6. Note that the E-field antenna channel A/D converter was in saturation for approximately 16 seconds and the noise power throughout the P-Static conditions (while the aircraft was flown through the snow cloud) was greater than 37 dB.

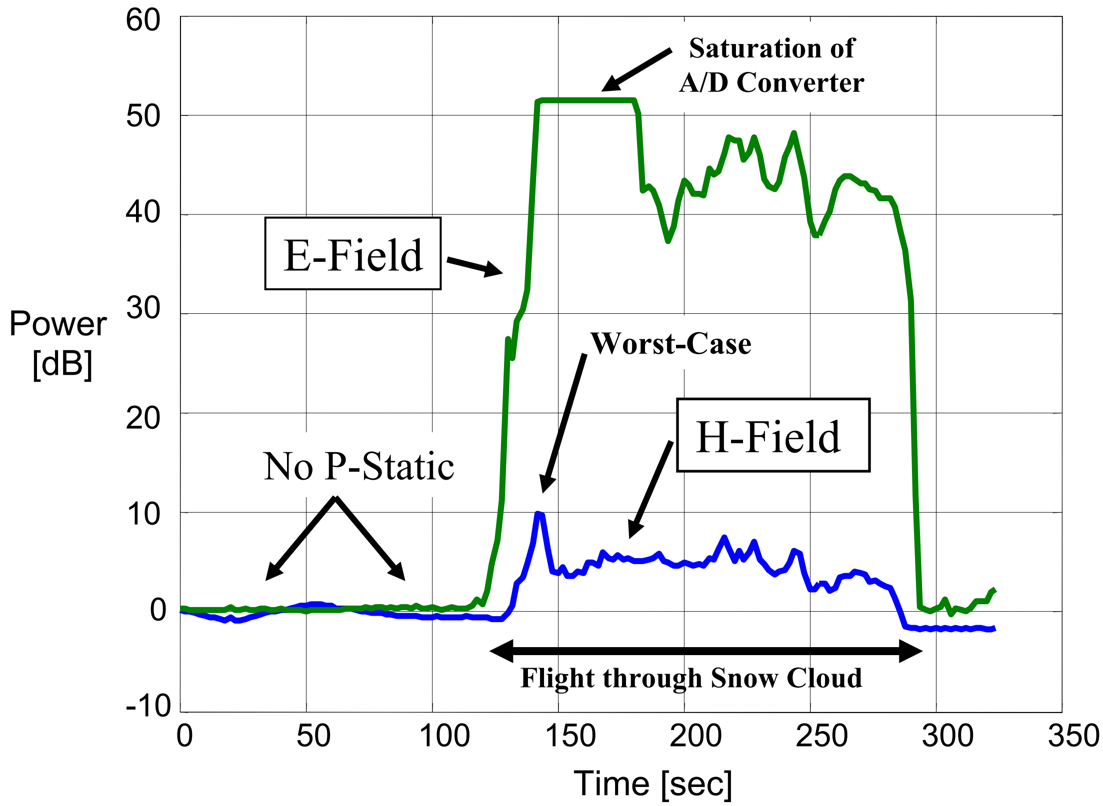

Figure 7.6 E-field and H-field received noise power relative to no P-Static conditions for the third flight test

The worst case for the H-field antenna was at the instance when the E-field antenna channel A/D converter went into saturation. However, the pulsing frequency of the noise is approximately 2 kHz thus resulting in degradation of less than 1 dB. Therefore, in summary, the H-field antenna mitigates P-Static noise by 41 dB for this particular flight test.

Figure 7.7 shows the discharge rate for the E-field antenna channel. The discharge frequency was calculated for a pulsed interference with a duration of 100 μs or more. Note that the E-field antenna channel A/D converter was saturated in the middle half of the data set. Pulsing frequencies up to 3 kHz can be observed for the E-field antenna channel.

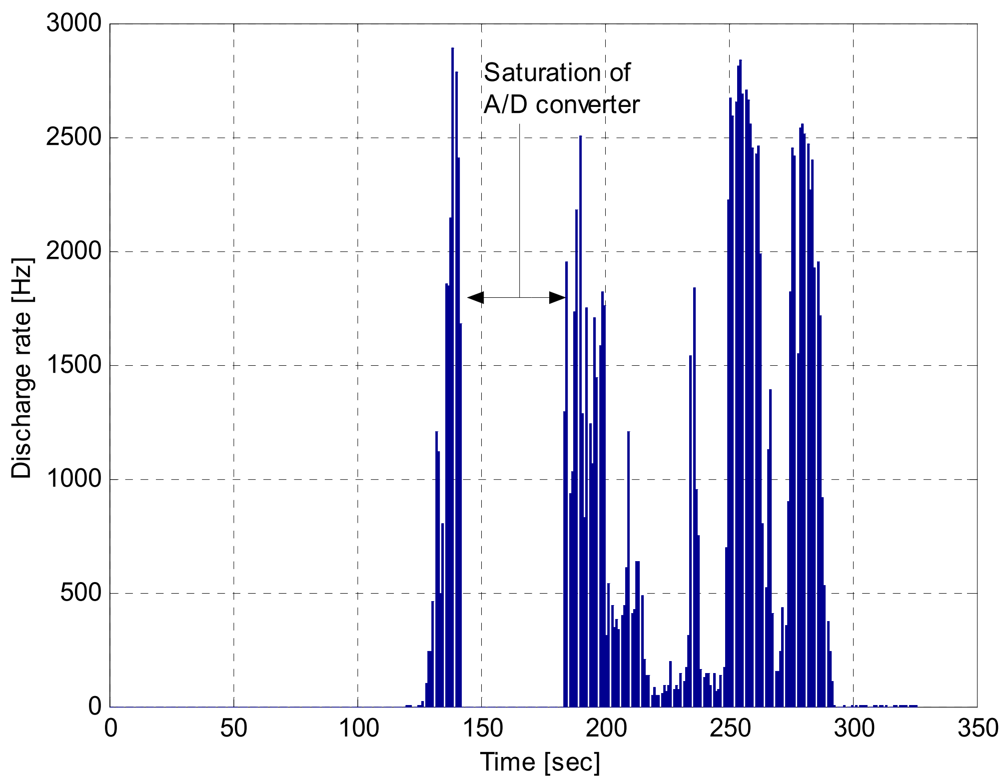

Figure 7.7 E-field antenna channel discharge rate for the third flight test

Discharge-rate calculations for the H-field antenna channel require additional processing that involves identifying and removing the Loran pulses from the pulsed interference. Further processing of the P-Static data is outside the scope of this thesis.

8 CONCLUSIONS

Based on the research described in this thesis, the following conclusions are drawn:

1. Distribution of noise (cores and tails) was determined for both E-field and the H-field antenna. The cores of the atmospheric noise distributions for both the antennas resemble a Gaussian distribution. The tail probabilities of both E-field and H-field antenna channel atmospheric noise can be overbounded by a Gaussian distribution with a standard deviation of about 3 to 3.25 times that of the collected data. Experimental data based on a sample size of approximately 130 million independent samples support these overbounds for probabilities as small as 10^{-6} to 10^{-7}. The shape of the cumulative distribution functions for both E-field and H-field antenna channels, under various conditions experienced in flight are similar.

2. E-field and H-field antennas are affected similarly by lightning-induced noise.

3. Loran can still be used in the presence of thunderstorm activity, with only a small increase in the received noise power. In the presence of thunderstorms, noise increase for both antennas was less than 2.3 dB. The cumulative distribution functions for the first and second flight tests (for both antennas) closely match in shape.

4. The P-Static data analyzed in this paper supports the anecdotal P-Static mitigation capability of the H-field antenna. An H-field antenna effectively mitigates aircraft Precipitation Static noise in the Loran-C band by more than 41 dB. An H-field antenna has greater immunity to high-voltage, low-current interference characteristics of P-Static than the E-field antenna. Moreover, it has an inherent 2 to 3 dB gain advantage over an E-field antenna. Thus, an H-field antenna can be used to achieve the availability and the continuity of the Loran-C navigation function.

9 RECOMMENDATIONS FOR FURTHER RESEARCH

It is recommended that the results obtained in this thesis be incorporated into the LORIPP process.

The flight data analyzed in this thesis did not process the StormScope data. Use of StormScope data along with the National Lightning Detection Network (NLDN) information would allow for comparison with the in-flight lightning-strike data. Use of a lightning locator data in conjunction the NLDN data would provide more information about the location of the thunderstorm with respect to the aircraft, thus giving a relation between the distance to the strike and the characterized noise.

Simultaneous collection of the ground and flight data under different weather conditions would give a better assessment of the ground and airborne noise.

The chain identification part of the processing software might not work well in presence of skywaves. Skywave interference has unpredictable signal strength and phase. In Alaska, for example skywave consideration is required to accurately identify Loran chains. Thus, skywave compensation should be an area of future work.

REFERENCES

1. LORAN-C User Handbook, COMDTPUB P16562.6, November 1992.

2. Van Graas, D.H. and Van Graas, F., "Aircraft Loran-C Dual-Loop Antenna System Design and Flight Test," Proceedings of the National Technical Meeting of the ION, San Diego, California, January 22-24, 2001.

3. Cutright, C., et al., "Loran-C Band Data Collection Efforts at Ohio University," Proceedings of the International Loran Association (ILA-32) Convention and Technical Symposium, Boulder, Colorado, November 3-7, 2003.

4. Lo, S., et al., "The Loran Integrity Performance Panel (LORIPP)," Proceedings of ION-GPS, Satellite Division of the ION, Portland, Oregon, September 24-27, 2002.

5. "Vulnerability Assessment of the Transportation Infrastructure Relying on the Global Positioning System," John A. Volpe National Transportation System Center, August 20, 2001.

6. Offermans G., and Helwig A., "Integrated Navigation System Eurofix - Vision, Concept, Design, Implementation and Test," Ph.D. Dissertation, Delft University of Technology, 2003.

7. Department of Transportation, United States Coast Guard, "Specification of the transmitted Loran-C Signal," Report COMDTINST M16562.4, Washington, D.C., July 1981.

8. Department of Defense and Department of Transportation, 1999 Federal Radionavigation Plan, February 2000.

9. Anderson, D., and Doty, J., "GPS-IMU-Loran Integration for Airborne Applications," Proceedings of ION NTM 2004, San Diego, California, January 26-28, 2004.

10. Feldman D., "An Atmospheric Noise Model with Application to Low Frequency Navigation Systems," Ph.D. Dissertation, Massachusetts Institute of Technology, June 1972.

11. Van Graas, F., "Electronic Navigation Systems I" and "Electronic Navigation Systems II" Course Notes, School of Electrical Engineering and Computer Science, Ohio University, Athens, Ohio, Winter 2003 and Spring 2003.

12. Lad, M., et al., "Characterization of Atmospheric Noise in the Loran-C Band," Proceedings of the International Loran Association (ILA-32) Convention and Technical Symposium, Boulder, Colorado, November 3-7, 2003.

13. Erikson, R., and Lilley, R., "FAA Tests an H-field Antenna to Increase Loran-C Availability During P-static Events," Proceedings of the International Loran Association (ILA-32) Convention and Technical Symposium, Boulder, Colorado, November 3-7, 2003.

14. Nickum, J. D., "The Effect of Precipitation Static and Lightning on the Airborne Reception of Loran-C," Volume I, Analysis, Avionics Engineering Center, Ohio University, Final Report, Report No. DOT/FAA/RD-82/45-1, prepared for U.S. Department of Transportation, Federal Aviation Administration, Washington, D.C., April 1982.

15. Edwards, J., "Results of Preliminary Flight Evaluation Comparing the Performance of H-field and E-field Loran-C Antennas in the presence of Precipitation Static," Technical Précis No. 281, Avionics Engineering Center, Ohio University, April 2000.

16. Lilley, R., and Burhans, R., "VLF P-Static Noise Reduction in Aircraft," Volume I: Current Knowledge," Avionics Engineering Center, Ohio University, Final Report, Report No. FAA-RD-80-137-I, prepared for U.S. Department of Transportation, Federal Aviation Administration, Washington, D.C., September, 1980.

17. "Vulnerability Assessment Of The Transportation Infrastructure Relying On The Global Positioning System," John A. Volpe National Transportation Systems Center, August 29, 2001.

18. Roth, L., and Schick, P., "Loran Receiver Technology: Yesterday, Today and Tomorrow," Proceedings of the International Loran Association (ILA-27) Convention and Technical Symposium, Danvers, Massachusetts, October 11-15, 1998.

19. Smith, A., Radio Frequency Principles and Applications: The Generation, Propagation, and Reception of Signals and Noise, IEEE press New York, 1998.

20. Offermans, G., Reelektronika's DataGrabber LORADD-DS: User installation and operation manual, Reelektronika b.v., November 29, 2002.

21. Van Graas, F., et al., "Loran-C P-Static," Briefing, Avionics Engineering Center, Ohio University, Athens, OH, April 30, 2004.

22. Boyce, L., et al., "A Time Domain Atmospheric Noise Level Analysis," Proceedings of the International Loran Association (ILA-32) Convention and Technical Symposium, Boulder, Colorado, November 3-7, 2003.

23. Uman, M. A., The Lightning Discharge, Dover Publications, Inc., Mineola, NY, 2001.

24. Peterson, B. et al., “Hazardously Misleading Information Analysis for Loran LNAV,” Proceedings of the International Symposium on Integration of LORAN-C/Eurofix and EGNOS/Galileo, June 2002.